

SUMMARY REPORT

TRANSIENT AND STEADY PERFORMANCE OF AN ION ROCKET
THRUST AUGMENTOR

prepared for

NATIONAL AERONAUTICS AND SPACE ADMINISTRATION

December, 1964

GRANT Na G-570

Technical Management
NASA Lewis Research Center
Cleveland, Ohio
Electric Propulsion Office
John Ferrante



U18401 0594912

TRANSIENT AND STEADY PERFORMANCE OF AN ION ROCKET THRUST AUGMENTOR

SUMMARY

The grant for the year 1964 included the design, construction and operation of a vacuum facility to do research on ion propulsion units. A cesium contact ion source with an electrostatic accelerator was also designed, constructed and put in operation. A thrust augmentor system is incorporated in the accelerator system. Preliminary measurements of the ion propulsion system in operation have been made.

A theoretical study of the acceleration of ions due to counter-current electron flow and secondary electron emission at the ion emitter has been made. The assumed model and solution indicates an increase in ion beam power is possible. However, the solution failed to give increases in ion beam power, equivalent to those observed experimentally.

A literature survey of the emission of secondary electrons has been prepared. Both the theoretical and experimental data reported on secondary electron emission at metal surfaces have been reviewed. An experimental program is underway to evaluate the secondary electron emission from porous tungsten ionizers.

INTRODUCTION

The present research program is directed toward understanding and improving the present state of the art of electrostatically accelerating ions. Present ion accelerator systems are limited by space charge effects. Maximum efficiency of an ion rocket would be obtained if it could be operated ion-limited rather than space-charge-limited. In other words, at present it is not always possible to accelerate all ions produced. A possible technique for overcoming the space charge limiting condition is to introduce electrons into the accelerator system. A single set of crude data was reported, ref. 1, which did indeed suggest that electrons can greatly improve the acceleration of ions.

The first phases of the research program at CSU are reported in this paper. An experimental facility was designed, built and put into operation during the first year for the grant. A cesium contact ion rocket with provisions for the injection of electrons was also operated on a trial basis. Further work on the development of a practical rocket for the experimental study is now in progress.

A theoretical model to explain the acceleration of ions due to the counter flow of electrons is also being sought. Previous study, ref. 2, failed to indicate increases of the order experimentally observed. Thus a theoretical model based on the emission of secondary electrons from the ionizer surface was investigated during the first years' grant. The result of this study still does not give power increases as great as those observed. Further evaluation of the theoretical analysis will be necessary in order to explain the results. Apparently the use of a non-interacting steady state ion-electron flow model may be too simple for the problem.

Work is also underway to evaluate the production of secondary electrons at the ionizer. The evaluation of secondary electron emission from a porous tungsten, cesium coated ionizer is now beginning. A general literature review of secondary electron emission is included as a part of this report.

I. Vacuum Facility

The 4 foot diameter by 15 foot long, vacuum chamber built during the present grant period is shown in figures 1. The chamber is now in routine operation. Under ideal conditions the chamber can be evacuated to less than 3×10^{-7} torr in approximately 1 1/2 hours starting at atmospheric pressure. With an ion engine in operation and probes actuated through the vacuum seals, the operating pressure is usually in the 10^{-6} torr range. The operations manual for the chamber is included as appendix A of this report.

II. Cesium Contact Ion Propulsion System

As outlined in the interim report, ref. 3, a porous tungsten-cesium contact ion propulsion system was designed for the experimental study. Figure 2 is a photograph of the completed system. The complete system is mounted with ceramic insulators on a brass plate. The brass plate is in turn mounted on two rails with small ceramic insulators. The brass mounting plate is, thus, insulated both from the voltages applied to the system and also from ground potential. In this way the breakdown of accelerator voltages to ground potential requires the failure of two insulators. The porous tungsten ionizers were shown in ref. 3. Evaluation of the properties of the ionizer is still in progress. First attempts to measure the volume flow rate through the ionizers gave unrealistic values for the porosity. These measurements are being repeated with improved measuring instruments.

Limited data on the operation of the ion system has been obtained in the preliminary tests. Figure 3 is a typical set of data plotted as cesium ion current density versus cesium reservoir temperature curve. The ionizer temperature was approximately 1660⁰F for the data shown.

As may be seen in figure 3 a condition of space-charge-limited flow was obtained for the + 1K, -2K volt condition. Figure 4 compares the ion current density obtained for the low temperature operating conditions with data reported by Kuskevics and Thompson, ref. 4, for similar ionizers. The extrapolated agreement indicates that the porous tungsten ionizers are operating as expected.

The major difficulty encountered in operating the ion system has been the development of the ionizer heater. First attempts used tantalum heater wires imbedded in a ceramic material, Rokite A which is a sprayed alumina coating. Difficulty was encountered in making connections to the tantalum wire. Secondly, the ceramic did not adhere to the ionizer block after several thermal cycles. The tantalum wire became brittle after it was heated and could not be further worked. The tantalum heater wire was replaced in later versions by tungsten - 26 per cent rhenium wire. The 73 W-26 Re wire can be silver soldered to connections and remains ductile after repeated thermal cycles. The ionizer heaters are now swaged in a 0.06 inch diameter metal sheath. Small ceramic (MgO) insulators are placed in the metal sheath and a 0.013 inch diameter 73 W-26 Re wire is threaded down the middle of the sheathed insulators. Both tantalum and stainless steel have been used as sheath material. Tantalum sheathes became very brittle. The stainless steel melts at temperatures slightly greater than 2000°F. Tungsten - Rhenium sheath material will be employed for future heaters, however, this material costs approximately \$10 per inch which means that approximately \$120 per heater will be invested.

The insulator material, MgO, for the heater will hold a potential difference of only 30 volts at 2000°F. Thus, it is necessary to make the heaters of low resistance (1 ohm or less) to prevent arcing from the heater wire to the ionizer block which leads to failure. The heaters have been operated at 10 amps without difficulty, as long as the voltage does not exceed approximately 30 volts.

The most important point in improving the ionizer heater was the radiation shielding. Without shielding, two hundred watts were required to reach temperatures of only 1250°F at the emitter. By adding a tantalum radiation shield around the heater and ionizer block, the power required to reach 1250°F was reduced by a factor of 3. The radiation shield was made of 0.005 inch thick tantalum sheet. The front of the sheet formed the focusing electrode of the emitter. A second improvement in radiation shielding was the addition of a ceramic powder to the space between the heater and the radiation shield. Figure 5 shows the actual measured improvement obtained by the radiation shielding.

III. Thrust Augmentor

The thrust augmentor tested in the initial experimental studies is shown in the photograph of figure 6. It is a 0.01 inch diameter thoriated-tungsten wire which was used to produce electrons in the accelerator region. As the study progresses the thoriated-tungsten wire will be replaced with a pure tungsten wire, so a better controlled supply of electrons will be available.

The initial run of the electron emission thrust augmentor was limited by malfunction of the cesium reservoir heater. The reservoir could be heated to only 400°F , thus for most of the practical measurements the system was ion limited rather than space charge limited. Figure 7 shows some of the metered data taken during the initial run. Figure 7a is a block diagram of the electrical hook-up of the system. In figure 7a the current density is plotted as a function of cesium reservoir temperature.

Figure 7c shows the effect of varying the electron emission wire voltage without emitting electrons. Figure 7d shows the effect of varying the electron emission wire voltage while maintaining a constant emission between 8.6 and 9.0 milliamps of electrons. The limited reservoir temperature makes it impossible to draw definite conclusion from this preliminary data.

A theoretical analysis of a simple model of the thrust augmentor was made for the research grant. This analysis is presented as Appendix B of this report. The results of this analysis suggest that an adequate model to explain the physical observations is still lacking. Further development of the model will await more experimental measurements.

IV. Instrumentation

A group of three instruments have been developed to analyze the ion beam; a) Hot Wire Calorimeter, b) Ion Energy Analyzer, and c) Floating Emission Probe. Because of the limited operation of the ion system to date, no actual ion beam measurements have been recorded with the instruments.

A. Hot Wire Calorimeter. - Construction of the hot wire calorimeter was outlined in ref. 3. Figure 8 shows the actual probe mounted in the vacuum chamber. The sensing element is a platinum - iridium wire, 0.0004 inches in diameter and approximately 0.10 inches long. The sensing element is roughly half the length of the wires used in the original development of the calorimeter, ref. 5. The wire was shortened to reduce the radiation error encountered with the longer wires. The short wire and cooling directly at the support tips greatly reduce the background errors encountered in the original probe designs of ref. 5. The sensitivity of the wire, as determined from a calibration curve of R versus I^2 for the wire in the vacuum, as shown in figure 9, is roughly half that of the wire used in ref. 5. It remains to determine if this lesser sensitivity will be adequate for the present ion system.

The water cooled hot wire calorimeter is remotely actuated by the actuator shown on top of the vacuum chamber in figure 8. An uncooled hot wire calorimeter probe is also used in the measurements. The uncooled calorimeter is mounted to a rotating arm contained in the same mounting flange with the ion system. This uncooled calorimeter can be used to

survey the ion beam at distances from roughly 1 inch from the ionizer to distances up to 15 inches along the beam. This particular acutator system will be employed with the velocity analyzer and the floating emission probe.

B. Ion Energy Analyzer. - A energy analyzer, simular to that reported by Sellen, ref. 6, has been built for analysis of the present ion beam. A photograph of the analyzer is shown in figure 10. The electronic control of the two curved plates is still being developed. An attempt is being made to utilize the high voltage power supplies used to accelerate the ions to also supply the voltage to the analyzer plates.

C. Floating Emission Probe. - A floating emission probe built according to the specification of ref. 7 has also been constructed. Figure 11 is a photograph of this probe. The case of the probe was made of brass instead of stainless steel. Since the probe will be operated very close to the ion system it is expected that sputtered atom of the case material may get back to the ionizer. Thus, a metal such as brass or copper is preferred to stainless steel, since stainless steel materials would not necessarily melt when it deposited on the ionizer.

V. Secondary Electron Emission Study

A. Literature Survey. - A literature survey of both experimental and theoretical studies of secondary electron emission is given as Appendix C of this report.

B. Experimental Study. - A electron collector has been built to study the secondary emission from the porous tungsten ionizers. Figure 12 is a photograph of the collector. This collector is designed to evaluate the angular distribution of the secondary electrons. Provisions are also made to study the secondaries due to primary electrons striking at angles of incidence to the ionizer. The bell jar assembly where the secondary electron experiments are to be made is an integral part of the vacuum chamber.

CONCLUSIONS

The general research facility and instrumentation for the study of an ion rocket thrust augmentor was completed during the first year of the grant. The ion rocket system has been operated and preliminary data recorded. The preliminary operation of the ion system has led to normally expected difficulties, which are being solved at the present time.

REFERENCES

1. Sandborn, V. A. and Baldwin, L. V.; Hot Wire Calorimeter Study of Ion Production and Acceleration. AIAA Journal Vol. 2, No. 4, 1964.
2. Muller-Lubeck, K.; Uber Die Ambipolare Raumladungsstromung Bei Ebenen Elektroden. Lectschrift Fur Angewandte Physik, III. Band Heft II. -1951. See also Langmurs, I. ; The interaction of electrons and positive ion space charges in cathode sheaths. Physic, Rev. 33, 954 (1919).
3. Transient and Steady Performance of an Ion Rocket Thrust Augmentor. Interim Report, June, 1964 to NASA from Fluid Dynamics and Diffusion Laboratory, College of Engineering, Colorado State University, Fort Collins, Colorado.
4. Kuskevics, G. and Thompson, B. L.; Comparison of Commercial, Spherical Powder, and Wire Bundle Tungsten Ionizers. AIAA Journal Vol. 2, No. 2, 1964.
5. Baldwin, L. V. and Sandborn, V. A.; Hot-Wire Calorimetry: Theory and Application to Ion Rocket Research. NASA Technical Report R-98, 1961.
6. Sellen, J. M. and Shelton, H.; Transient and Steady State Behavior in Cesium Ion Beams. Electrostatic Propulsion, Vol. 5 Progress in Astronautics and Rocketry, Academic Press, New York, 1961.
7. Design, Development, and Fabrication of a Floating Embsive Probe for Ion Beam Diagnostics. Space Technology Laboratories, Inc. Report 9240-0186, 1963.

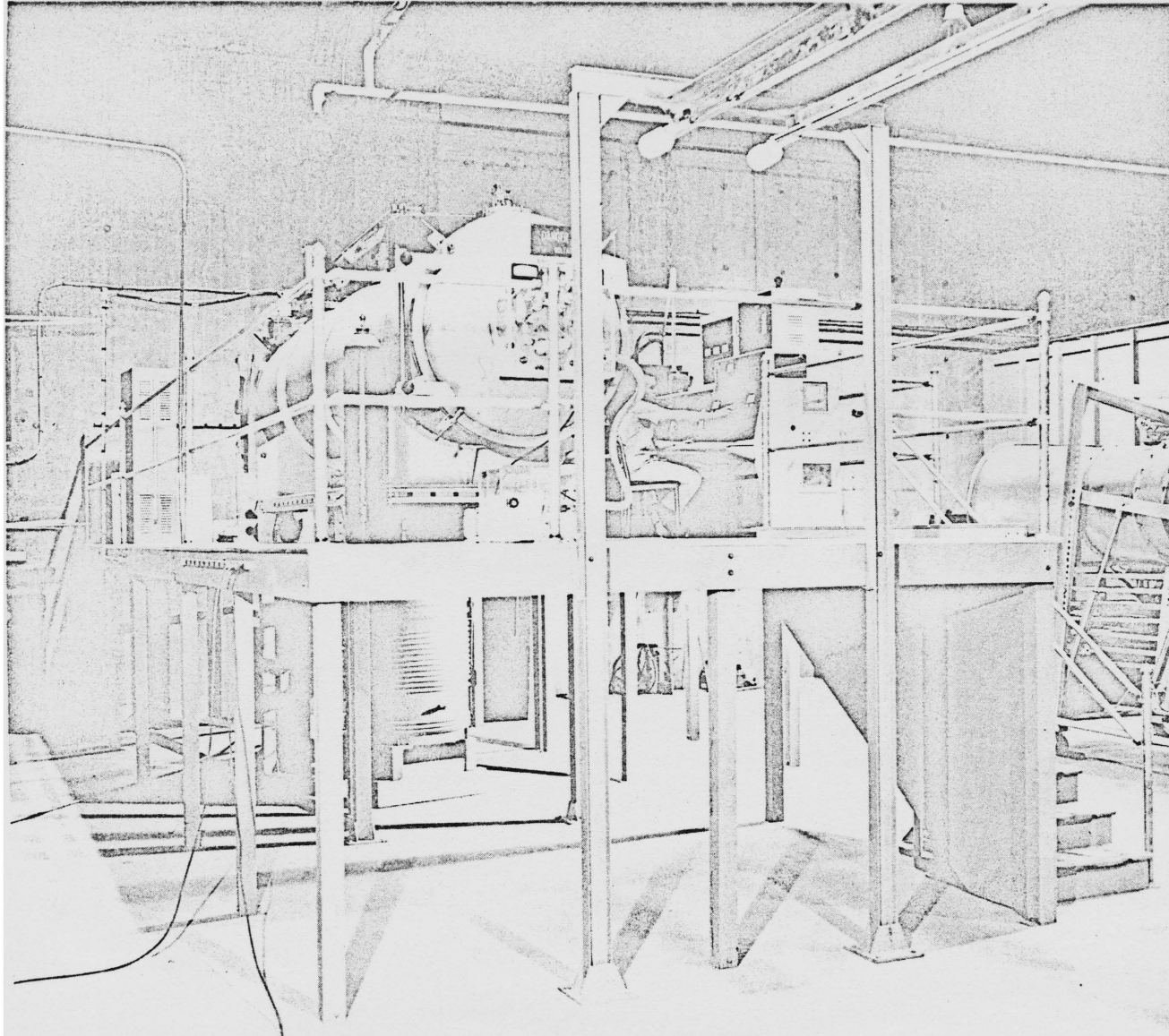


Figure 1. - CSU-NASA Ion Research Vacuum Facility

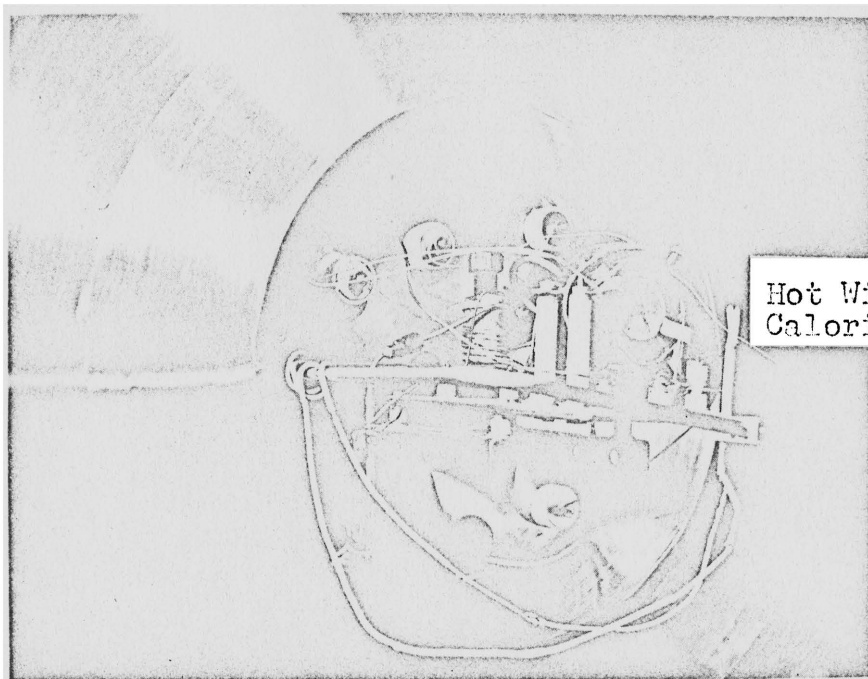
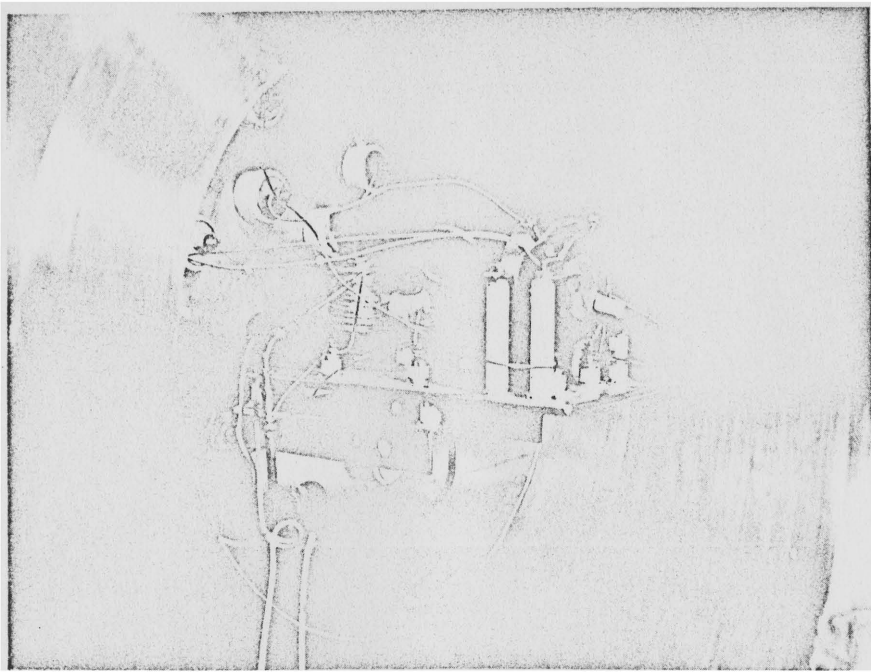


Figure 2. - Cesium Contact Ion Propulsion System

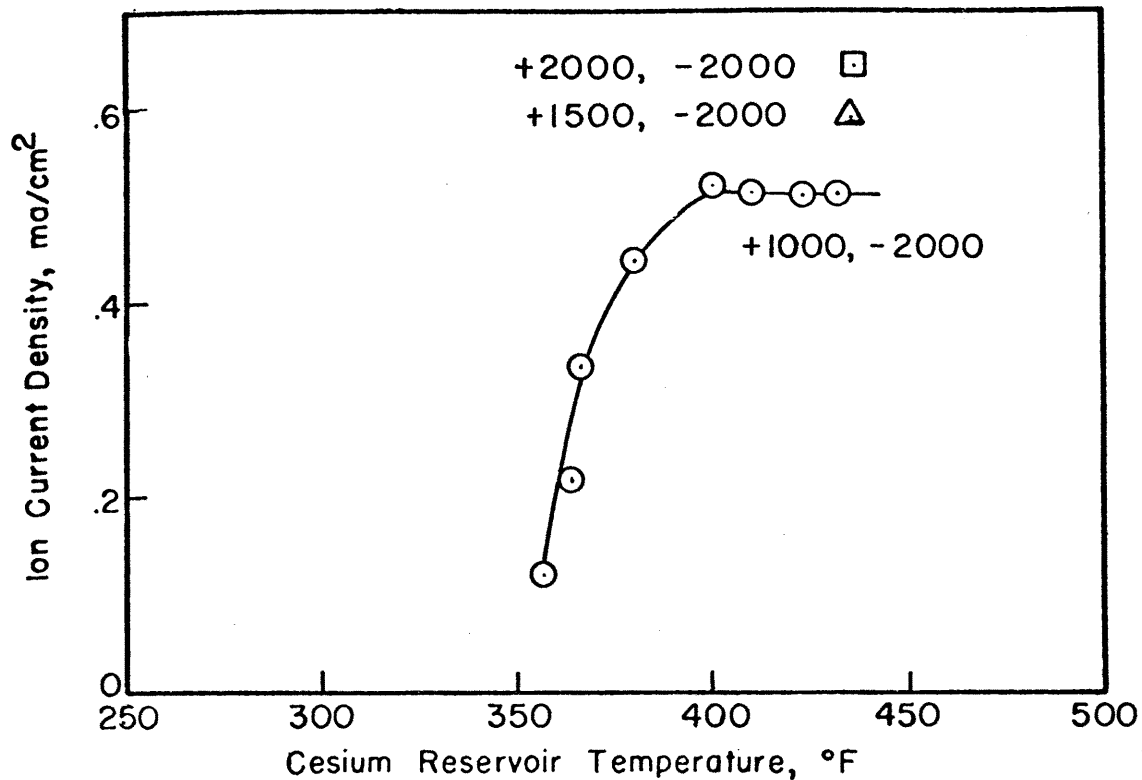


FIG. 3.- ION CURRENT DENSITY AS A FUNCTION OF CESIUM RESEVOIR TEMPERATURE. (IONIZER TEMPERATURE 1660 °F)

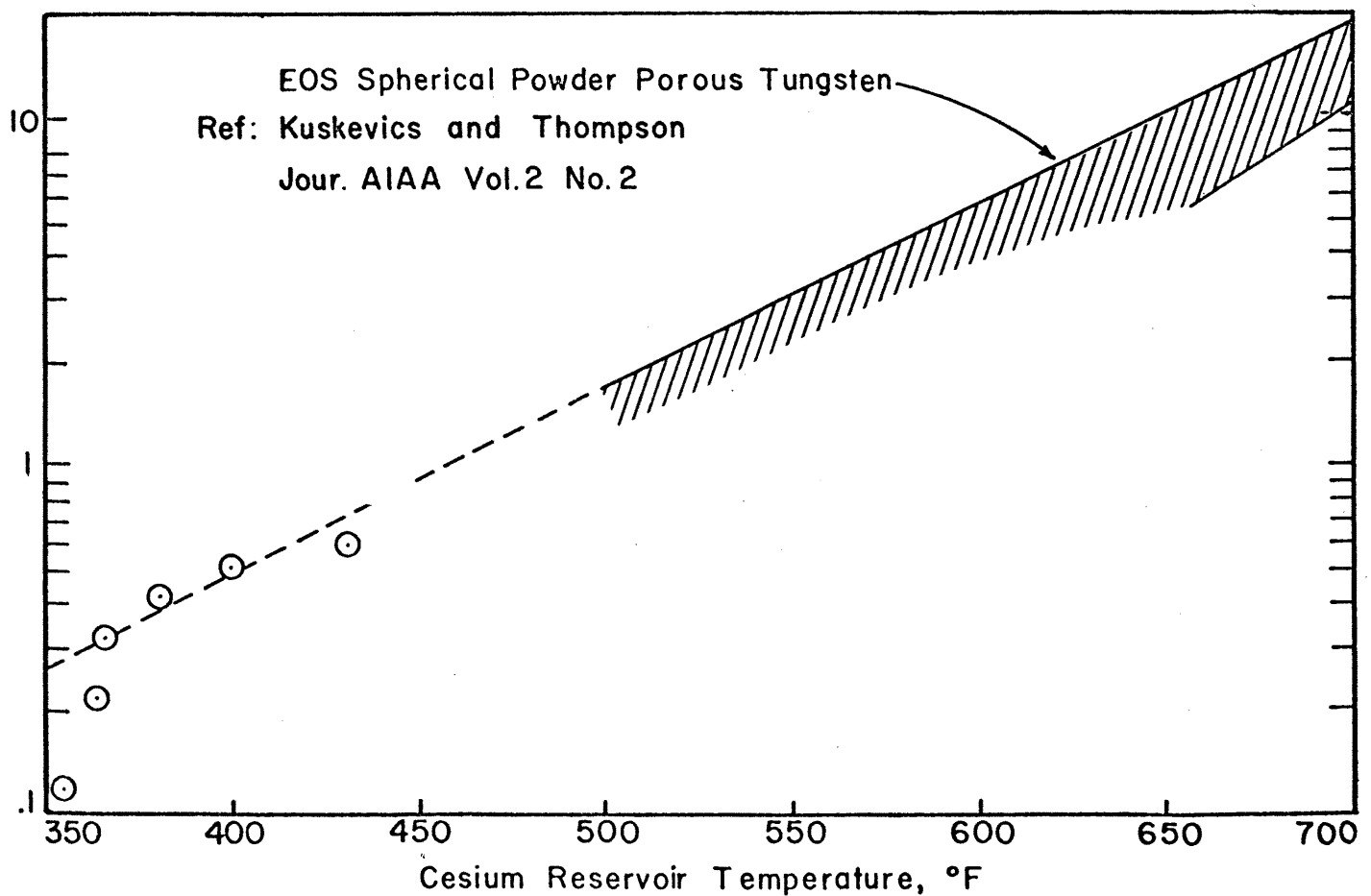


FIG. 4.- COMPARISON OF MEASURED ION CURRENT DENSITY WITH PREVIOUS REPORTED DATA.

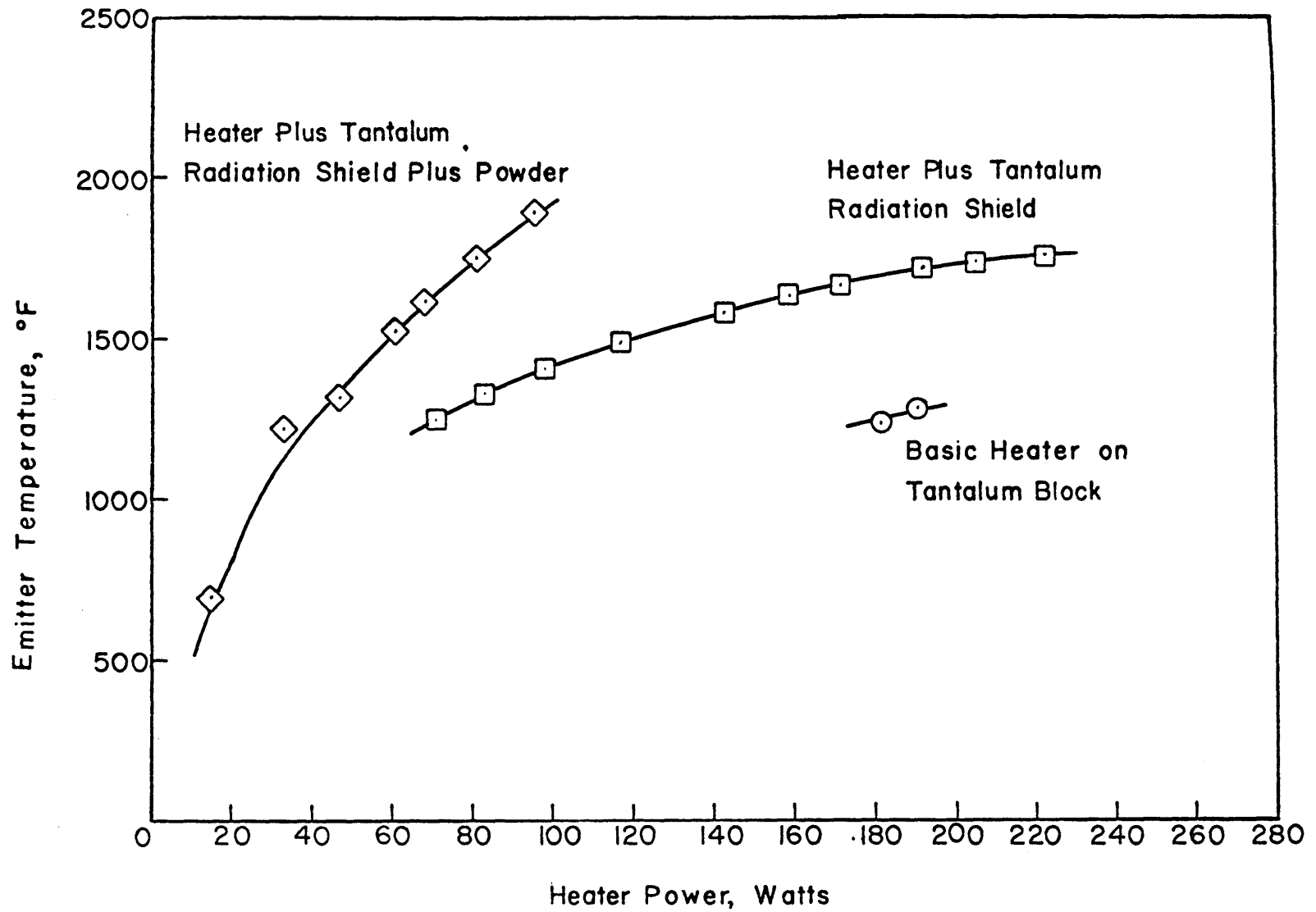


FIG. 5.- EFFECT OF RADIATION SHIELDING AND POWDER ON POWER REQUIRED TO HEAT THE IONIZER.

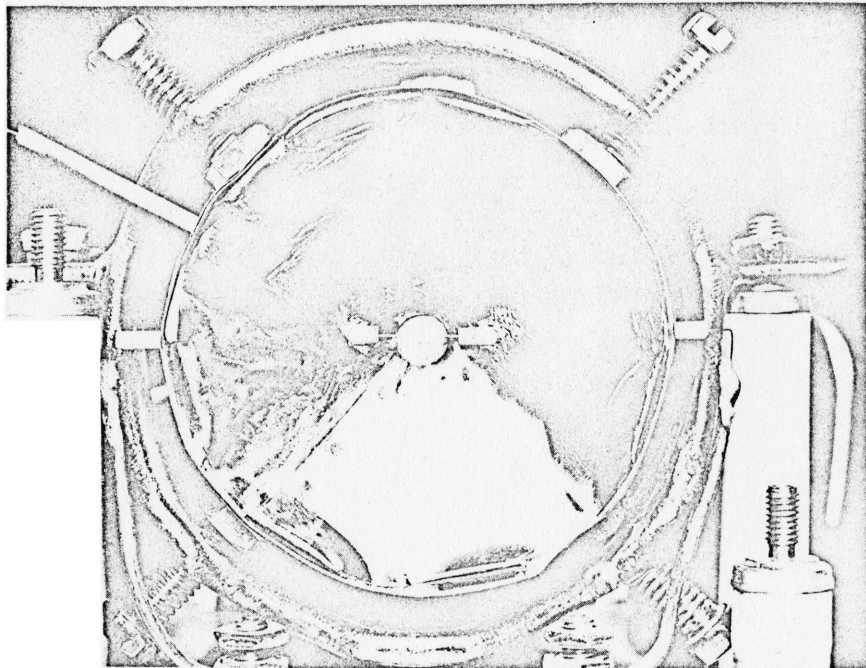
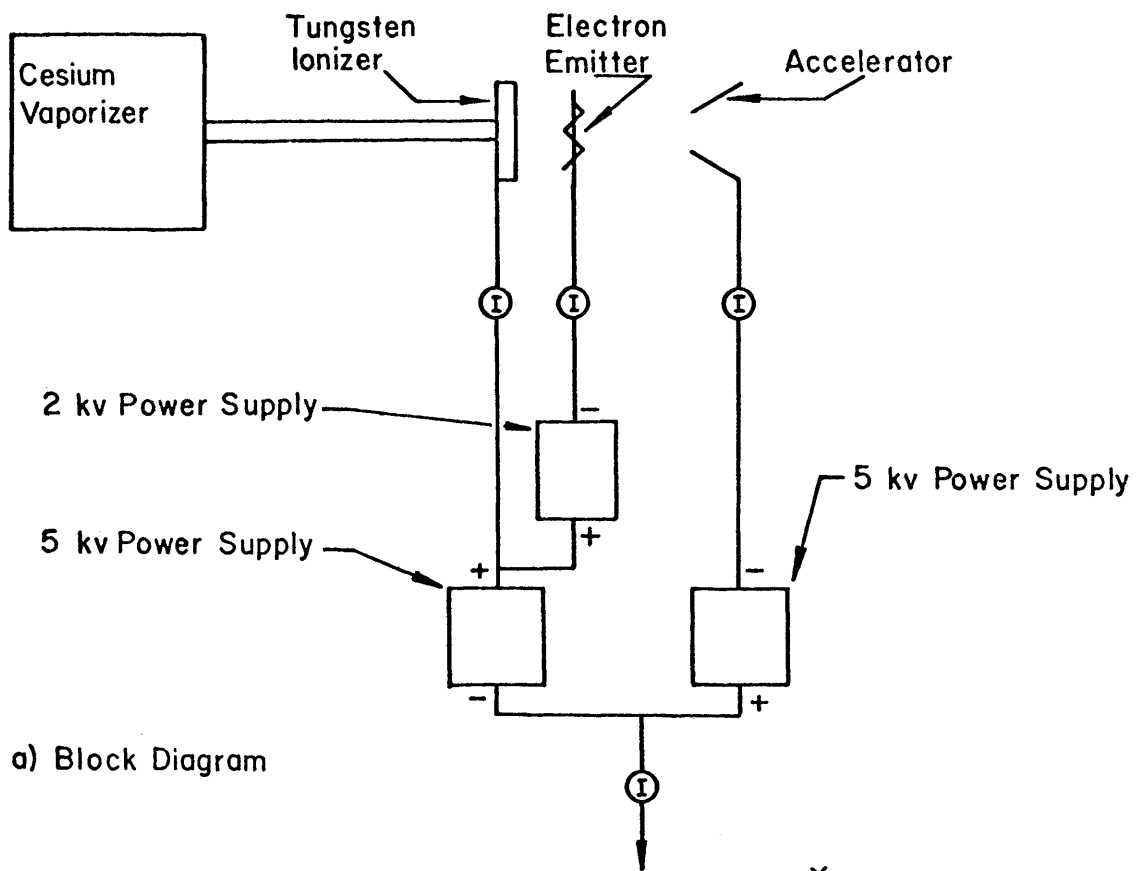
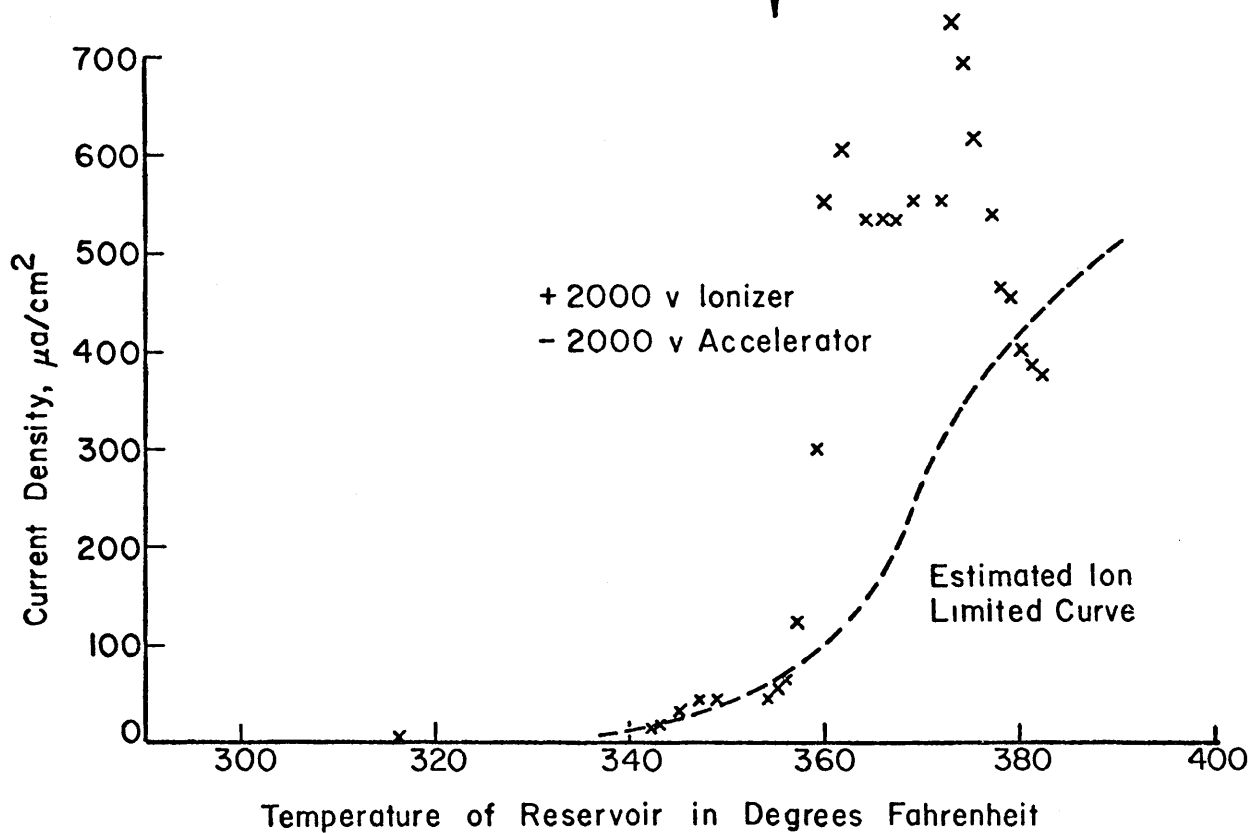


Figure 6. - Electron Emission Wire Across the Ionizer Face.



a) Block Diagram



b) Current Density Versus Reservoir Temperature. (No Forced Electron Emission)

FIG. 7. - OPERATION OF ION ACCELERATOR SYSTEM WITH AN ELECTRON EMITTER.

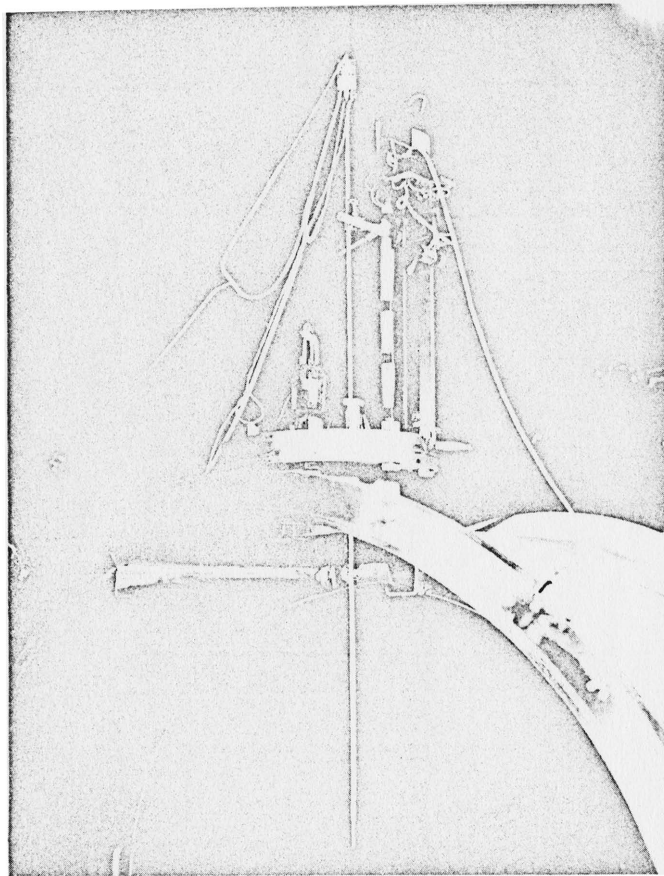


Figure 3. - Hot Wire Calorimeter Probe Mounted
in the Vacuum Chamber.

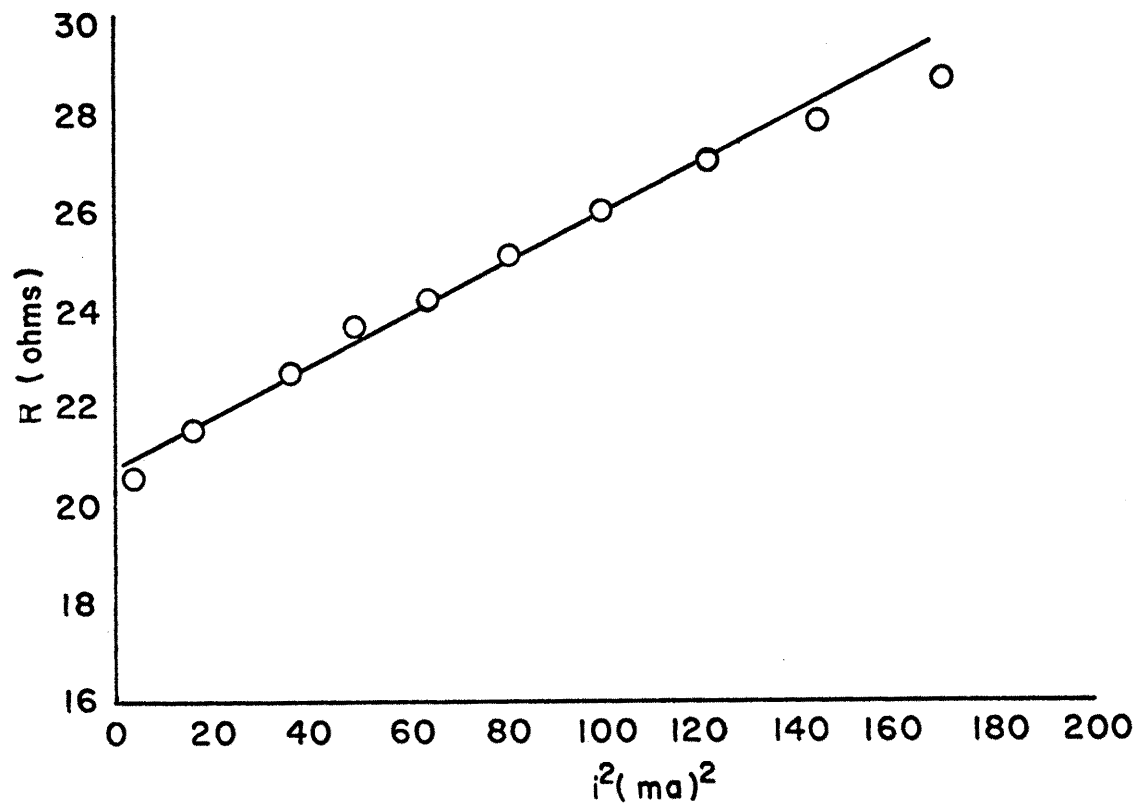


FIG.9 CALIBRATION CURVE FOR A HOT WIRE CALORIMETER

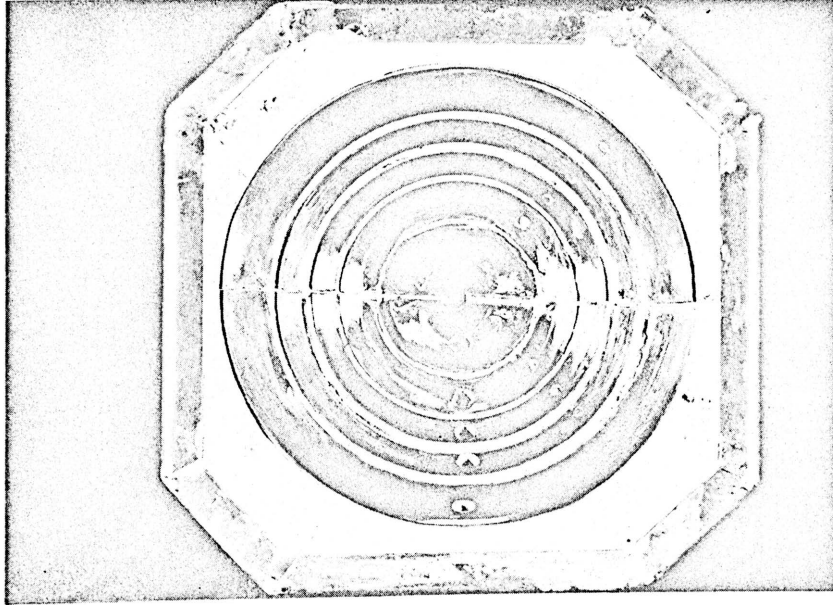


Figure 10. - Ion Velocity Analyzer.

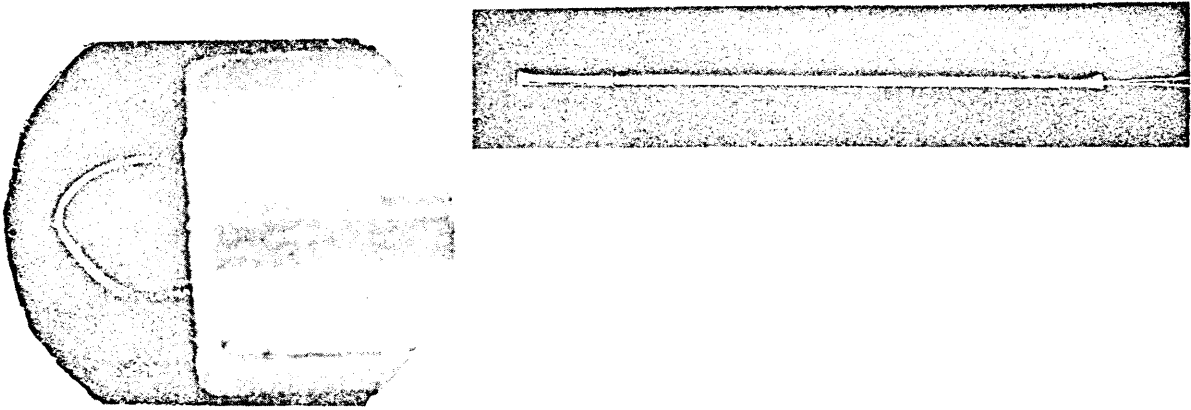


Figure 11. - Floating Emission Probe.

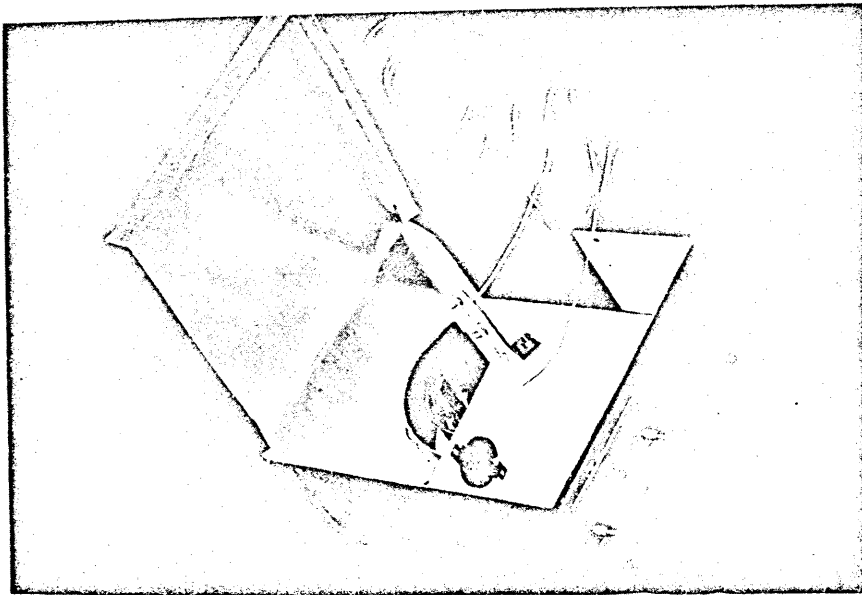
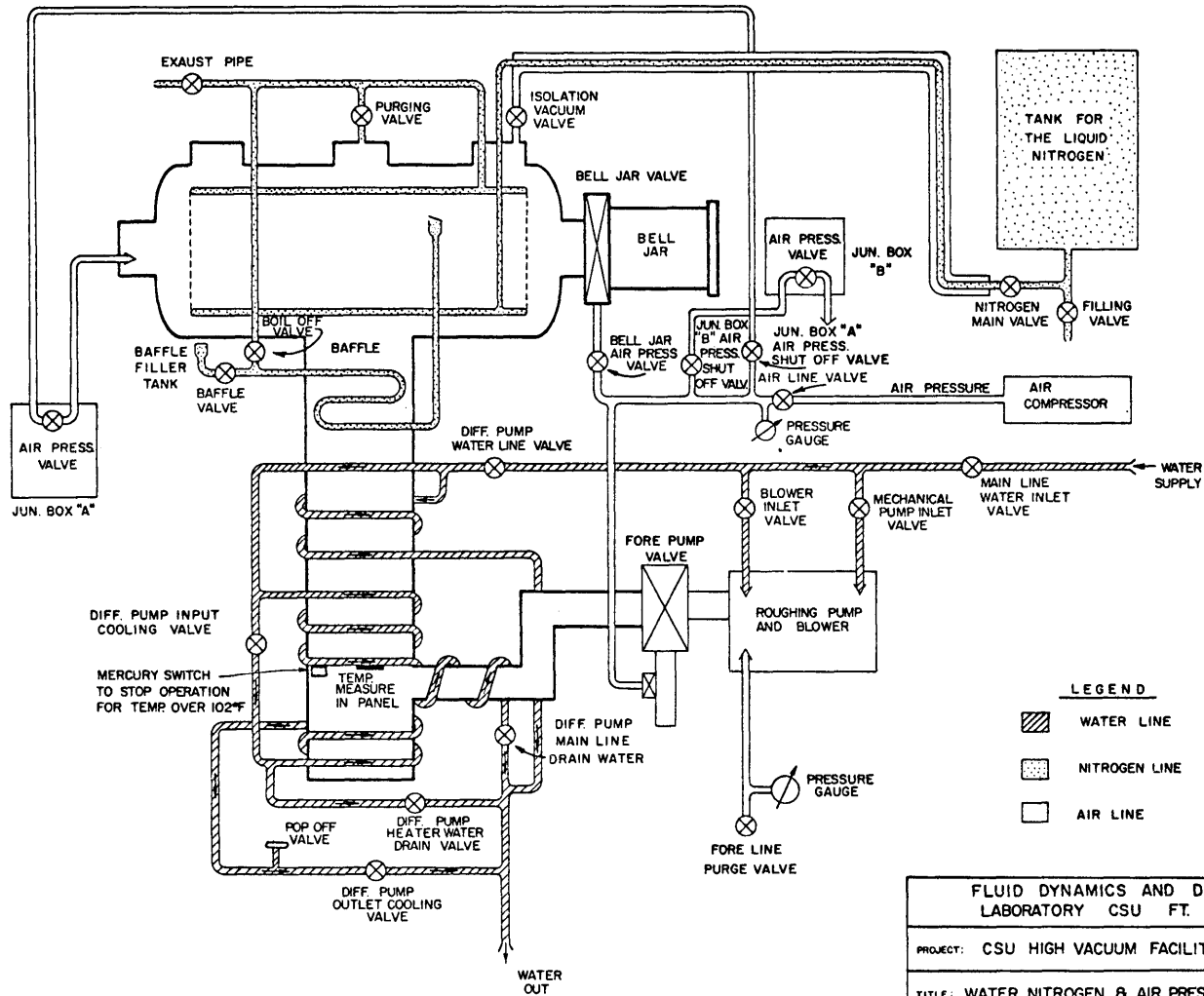


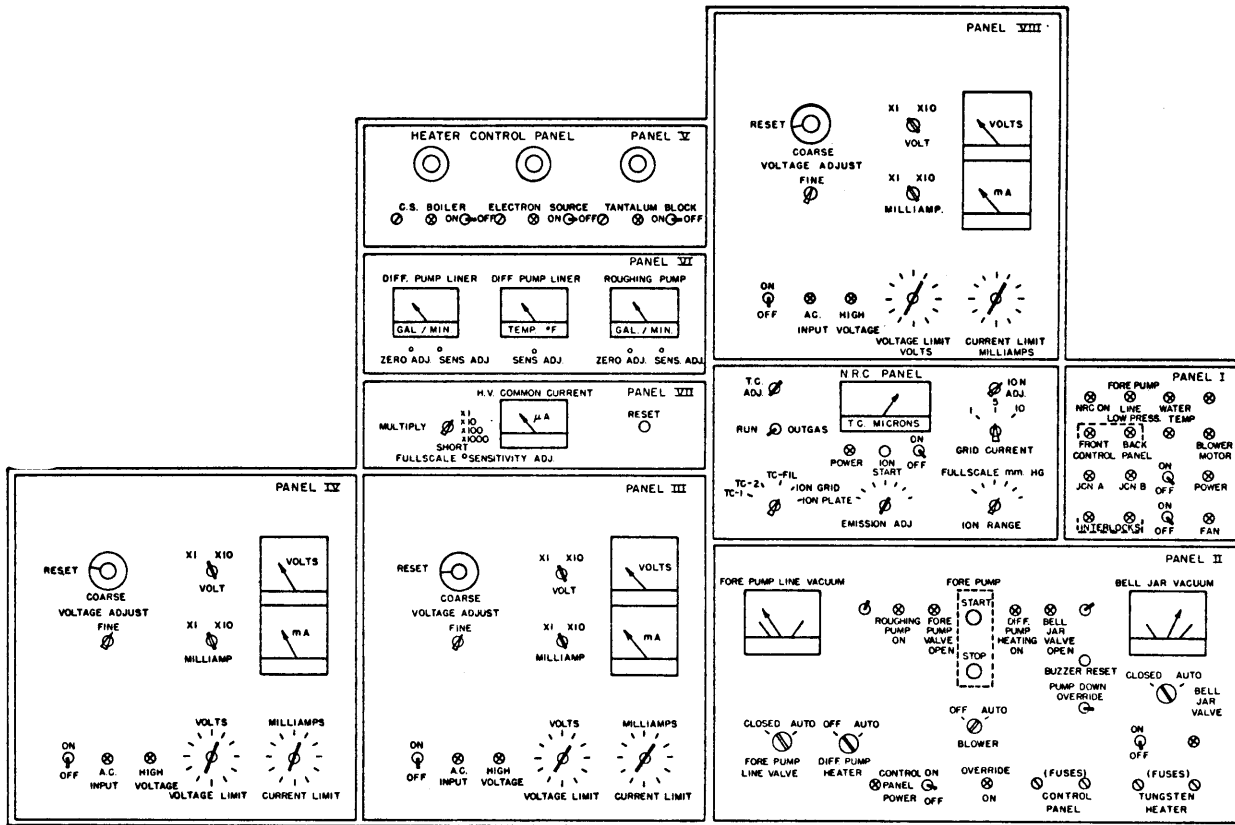
Figure 12. - Secondary Electron Collector.

FLUID MECHANICS AND DIFFUSION LABORATORY
COLORADO STATE UNIVERSITY
Fort Collins, Colorado

CSU HIGH VACUUM FACILITY
Manual of Operation and Schematics

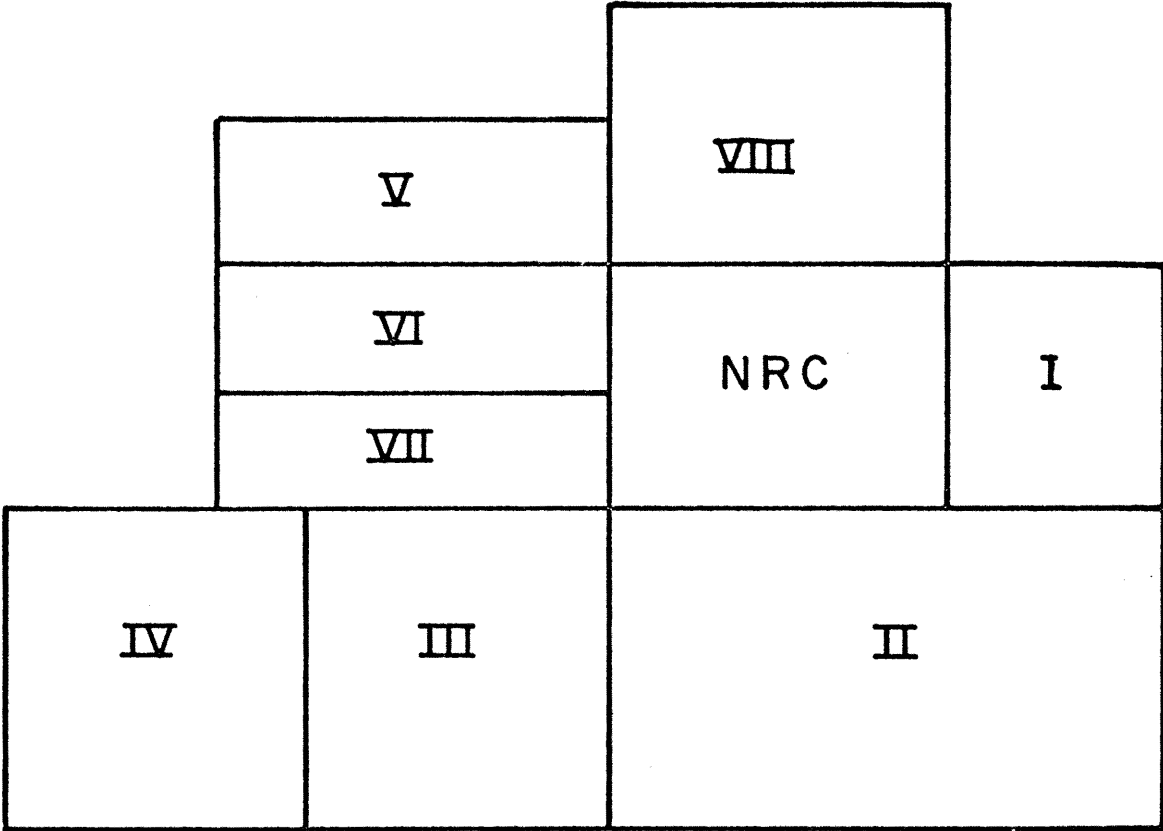
August 1964





FLUID DYNAMICS AND DIFFUSION LABORATORY CSU FT. COLLINS		
PROJECT CSU HIGH VACUUM FACILITY		PROJECT NO 1509
TITLE: PANELS DISTRIBUTION OF THE CONSOLE		
DESIGN BY L. W. MAXWEL	DRAWN BY HANAE AKARI	SCHEMATIC NO
DATE JULY 1964	DATE AUGUST 1964	

PANEL NUMBERS



BEFORE OPERATION

Before operation of the facility all the switches and indicators have to be set according to the following description:

PANEL I

All indicators, off

Interlock lights and switches, off

PANEL II

"FORE PUMP LINE VALVE" in "AUTO"

"DIFF PUMP HEATER" in "OFF"

"BELL JAR VALVE" in "CLOSED"

"BLOWER" in "AUTO"

"CONTROL PANEL POWER" in "OFF"

All indicators are off.

"FORE PUMP LINE VACUUM" meter: High Pressure

"BELL JAR VACUUM" meter indicating: High Pressure

NRC PANEL

Power switch in "OFF"

"POWER" indicator off

"METER SELECTOR" in "TC-2"

For adjustment and calibration of the NCR panel see NCR-Manual.

PANELS III, IV, AND VIII

"AC" switch in "OFF"

"AC INPUT" indicator off

For operation of these panels, see "High voltage supplies".

VACUUM, AIR and NITROGEN VALVES

Before starting the pump-down it is necessary to check if the valves for vacuum and cooling supplies are in the proper position. The following table may help for the check out of all valves:

<u>VALVE</u>	<u>LOCATION</u>
ISOLATION VACUUM VALVE , open	1. Tower on the tank
PURGING VALVE, closed	2. Tower on the tank
EXHAUST PIPE, closed	2. Tower on the tank
BAFFLE VALVE, open	West side of the tank
BELL JAR AIR PRESS VALVE, closed	Bottom of Bell Jar
AIR LINE VALVE, open	Left side of the console
MAIN VALVE (NITROGEN), closed	Outside of the building
FILLING VALVE, closed	Outside of the building
MAIN LINE WATER VALVE, open	Left side of the console

OPERATION (Pumping-down)

- 1) The first thing to do before the operation of the vacuum facility is to set the water valves properly for the cooling of the pumps. The sequence of setting the valves is as follows:

<u>VALVE</u>	<u>LOCATION</u>
Close the "DIFF PUMP INPUT VALVE"	Downstairs
Close the "DIFF PUMP OUTLET COOLING VALVE"	"
WARNING: If the next two valves are not open the water line may blow out!	
Open the "Drain Cock" of the "DIFF. PUMP OUTLET COOLING VALVE"	Downstairs
Open the "POP OFF VALVE"	"

OPERATION (Pumping-down)LOCATION cont'd"

Open the "DIFF PUMP HEATER WATER DRAIN VALVE" to drain water, when this line is empty close the valve. Downstairs

Open the "BLOWER INLET VALVE" Downstairs

Open the "MECHANICAL PUMP INLET VALVE" only 1-1/2 turns Downstairs

Permanent open have to be the "DIFF PUMP WATER LINE VALVE" and the "DIFF PUMP MAIN LINE DRAIN VALVE". Downstairs

2) CONNECTION OF THE AC LINES

Switch on the "110 MAIN DISCONNECT" switch, to supply power to the console and all AC outlets. Downstairs on the south wall of the building .

Switch on the "440 MAIN DISCONNECT" switch, to supply power to the diffusion pump heaters, roughing pump and blower. Downstairs on the south wall of the building.

Switch on the "110 CONSOLE SWITCH" (red) to supply power to the panels I, III, IV, and VIII. On the left side of the console.

Switch on the "440 CONSOLE SWITCH" to supply power to the pumps and blower. On the left side of the console.

OVERLOAD OF AC LINES

If some of the AC lines are accidentally overloaded, the "CIRCUIT BREAKER LOAD CENTER" open that circuit. The breakers are: On the left side of the console.

1 "Control panel plug mold front" under the console

4-5 "30 Amps for panels II and V"

OPERATION (Pumping-down) cont'd:LOCATION cont'd:

- 13 "Control panel plug mold back
(Back of the console)
- 14 "Plug mold south end", for all the south
plug molds of the facility.
- 15 "Plug mold north end" for all the north
plug molds of the facility.

Indicators on:

- 3) Switch on "CONTROL PANEL POWER". It switches on the power supplies of the instruments "CONTROL PANEL ON" in the panels
- 4) Switch in NRC-panel, the "METER SELECTOR" to "TC-2" position, "FULL SCALE mmHG" to "10⁻³"
- 5) Switch "ON" the NRC power switch NRC "POWER", "NRC ON"
- 6) Open "AIR LINE VALVE" for air pressure
The "AIR PRESSURE GAUGE" has to indicate between 70 and 80 psi.
- 7) Open "MAIN LINE WATER VALVE" and adjust valves to obtain at least: in Panel 6 for "DIFF PUMP LINER": 5 Gal/min and for the "ROUGHING PUMP": 2 Gal/min.
- 8) The temperature of the "DIFF PUMP LINER" has to be less than 100° F. Panel 6.
- 9) Depress "PUMP DOWN OVERRIDE" until valve is open and then depress "FOREPUMP START". Be sure that the mechanical pump (Roughing pump) turns counter clock wise looking at the pump west to east. This pump is downstairs.
"OVERRIDE ON"
"ROUGHING PUMP ON"
"FOREPUMP VALVE OPEN"
- 10) Set the upper and lower limits of the "FORE PUMP LINE VACUUM" meter.

OVERLOAD OF AC LINES cont'd:

Indicators on: cont'd

- 11) After a few minutes the blower will be automatically started. This usually takes 10 minutes when starting from atmospheric pressure in tank. "BLOWER MOTOR"
- 12) After a certain vacuum is reached, the "OVERRIDE ON" indicator will be off. The level where the "OVERRIDE ON" indicator turns off, depends on the upper limit set in the "FORE PUMP LINE VACUUM" meter.
- 13) When the "FORE PUMP LINE VACUUM" meter indicates the upper limit, the diffusion pump can be started but first it is necessary to follow the next steps in order to operate the nitrogen's cooling system. "WATER TEMP."
- 14) Open the "BAFFLE VALVE" and fill the baffle of the Diffusion Pump with liquid nitrogen. This can be obtained from the liquid nitrogen main tank outside of the building by opening the "FILLING VALVE".
- 15) The facility has to be operated for a longer time with the roughing pump and blower. The baffle has to be refilled continuously until the exhaust line of the baffle is completely frosted and the pressure in the facility goes down to about 3×10^{-4} mmHg.
- 16) Turn on the "DIFF PUMP HEATER" switch to "AUTO". "DIFF PUMP HEATER ON"

- 17) When the pressure is about 1.2×10^{-6} open the nitrogen line.
- 18) Close the "BAFFLE VALVE"
- 19) To operate the nitrogen line, open the "MAIN VALVE", outside of the building very slowly to approximately 1/2 turn. If too much nitrogen goes out in the "EXHAUST PIPE" turn the "MAIN VALVE" back to about 1/4 turn. This operation of opening more or less the "MAIN VALVE" has to be made many times during the operation of the facility to get the proper flow of nitrogen.

CLOSEDOWN OPERATION

Before increasing the pressure in the tank, it is very important to disconnect all the devices in the experiment that can be damaged by the higher pressures. It is also very important to be careful with the operation of the NRC-panel when the pressure in the facility increases.

LOCATION

- 1) Turn the "DIFF PUMP HEATER" switch to "OFF" Panel II
- 2) Open the "DIFF PUMP INPUT COOLING VALVE" very slowly avoiding too much cold water flowing in the lowest cooling circuit. At the same time steam will flow out from the "POP OFF VALVE" and the "Drain cock" of the "DIFF PUMP OUTLET COOLING VALVE". When too much cold water flows in the lowest cooling circuit, the high temperature of the lines will create steam (bubbles) and the operator can realize their presence by the noise it produces.

CLOSEDOWN OPERATION cont'd:LOCATION cont'd:

After 15 or 20 minutes water will flow out from the "POP OFF VALVE" and the "Drain cock of the "DIFF PUMP OUTLET COOLING VALVE", then

- 3) Close the "POP OFF VALVE" and the "Drain cock" of the "DIFF PUMP OUTLET COOLING VALVE", and at the same time open slowly the "DIFF PUMP OUTLET COOLING VALVE".

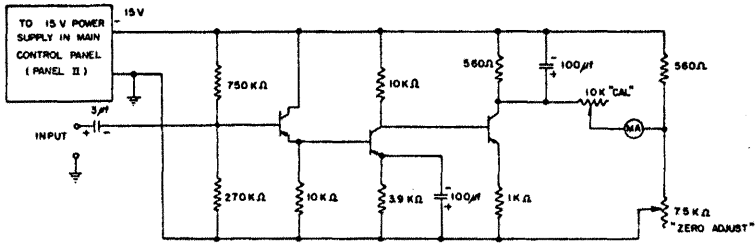
It takes approximately 2 hours until the temperature of the diffusion pump's heaters drops to about 200°F.

- | | |
|--|--------------------------|
| 4) Close the "NITROGEN MAIN VALVE". | Outside of the building |
| 5) Depress "STOP" in panel II, to turn off the mechanical pump and blower. | Panel II |
| 6) Close the "MAIN LINE WATER VALVE" | Left side of the console |
| 7) Close the "AIR LINE VALVE" | Left side of the console |

After following the above instructions it is possible to switch off the power in all the panels and equipments. It is strongly recommended to switch off the "110 CONSOLE SWITCH" (red) before touching or coming close to the high voltage connections of the facility. This switch disconnects the high voltage power supplies.

PURGING

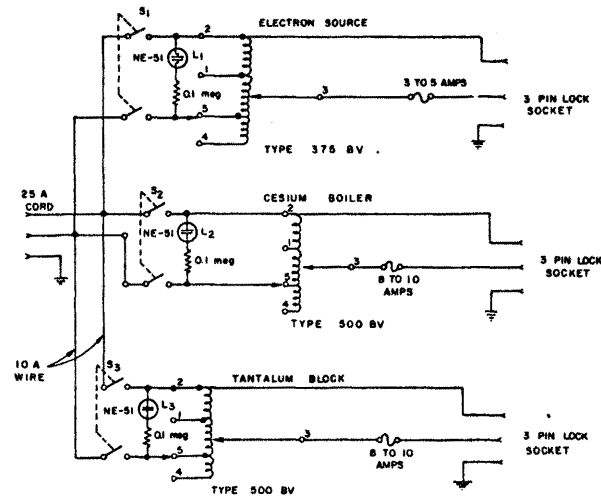
- | | |
|--|---------------------------|
| To let air into the tank open the "EXHAUST PIPE" | 2. Tower on the tank |
| Open the "PURGING VALVE" about 4 or 5 turns and after 15 minutes open it completely. | 2. Tower on the tank |
| Open the "FORELINE PURGE VALVE" | Left side of the console. |



FLOW METER AMPLIFIER

DESIGNED: JIM CLINE

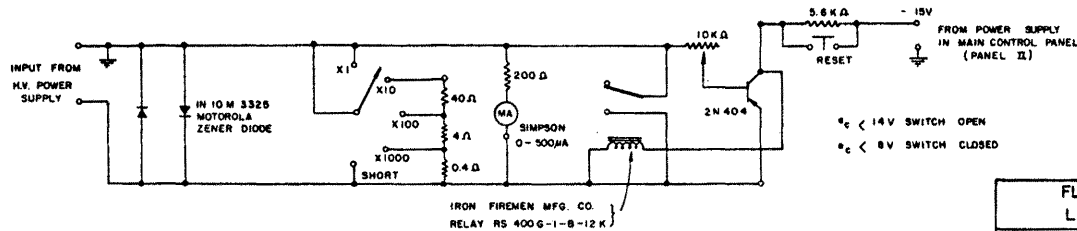
LOCATION PANEL VII



ION ENGINE SUPPLIES

DESIGNED: L.M. MAXWELL

LOCATION: PANEL V



*c < 14V SWITCH OPEN
*c < 8V SWITCH CLOSED

FLUID DYNAMICS AND DIFFUSION
LABORATORY C.S.U FT. COLLINS

PROJECT: CSU VACUUM FACILITY

PROJECT NO.
1509

TITLE: CONSOLE INSTRUMENT PANELS V, VI & VII

HV COMMON
CURRENT METER

DESIGNED: JIM CLINE

LOCATION: PANEL VII

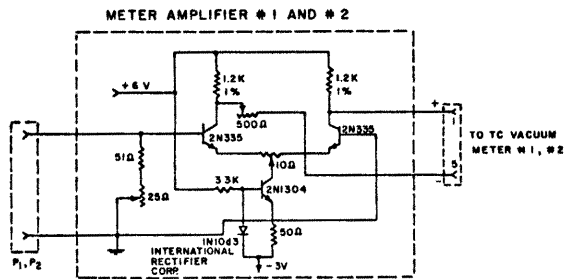
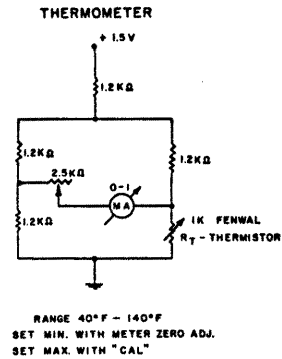
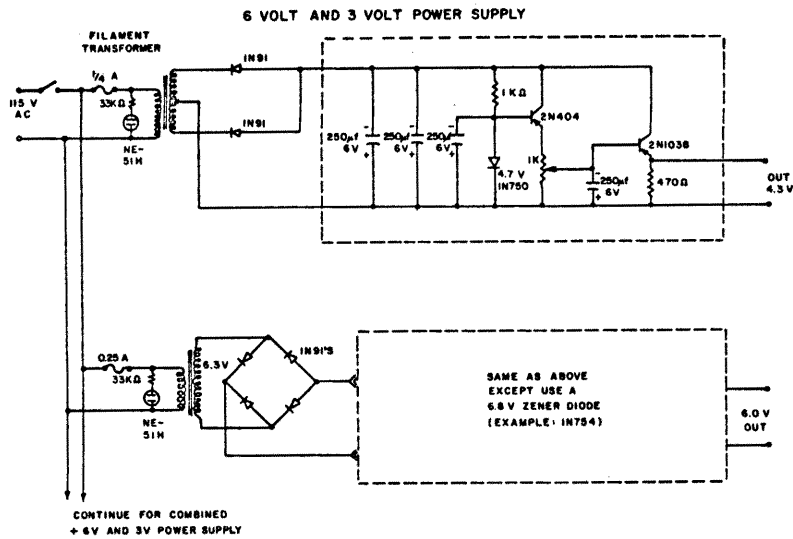
DESIGN BY: STAFF

DATE: JULY, 1964

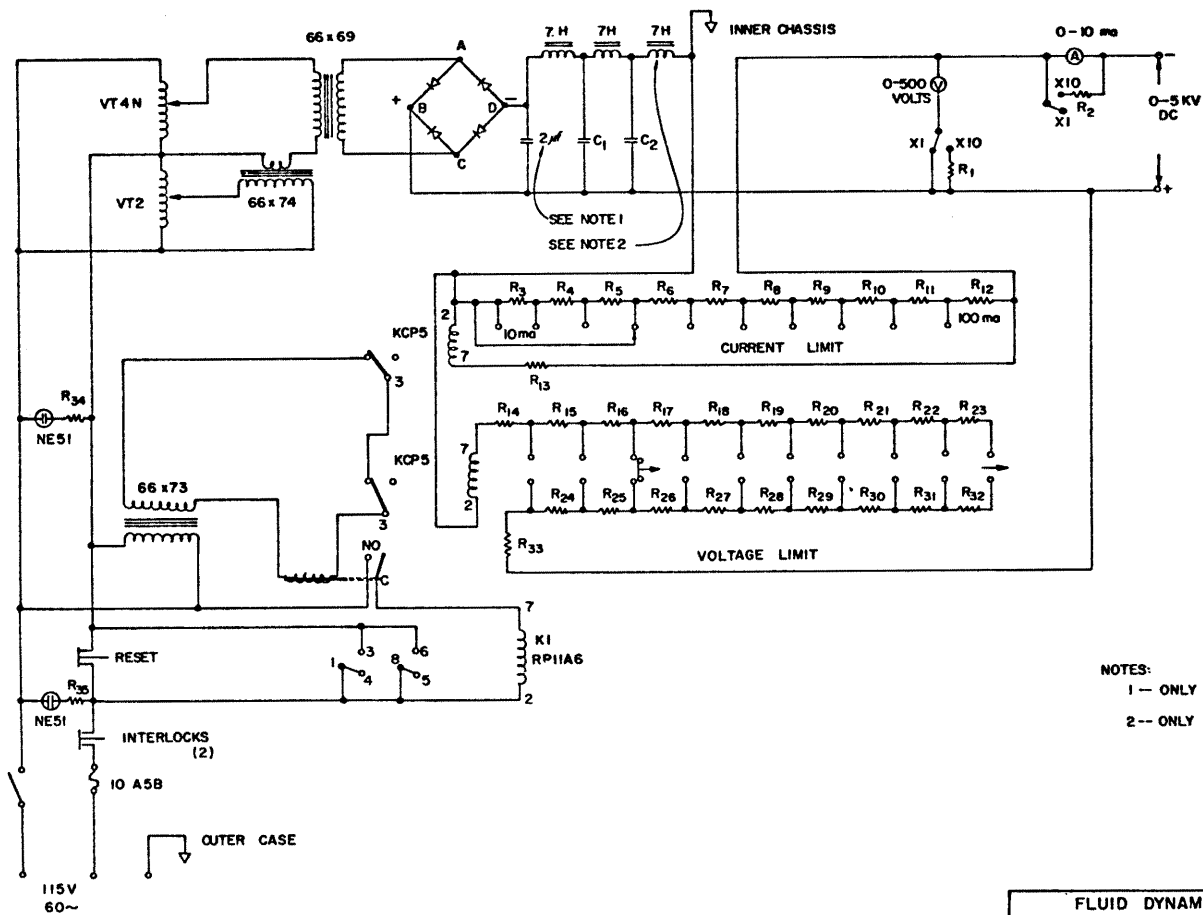
DRAWN BY: M. AKARI

DATE: AUGUST, 1964

SCHEMATIC NO.



FLUID DYNAMICS AND DIFFUSION LABORATORY C.S.U. FT. COLLINS		
PROJECT: C.S.U. HIGH VACUUM FACILITY	PROJECT NO. 1509	
TITLE: METER AMPLIFIER AND POWER SUPPLY		
DESIGN BY: <u>C. FINN</u>	DRAWN BY: <u>M. AKARI</u>	SCHEMATIC NO.
DATE: 8/12/64	DATE: 8/31/64	

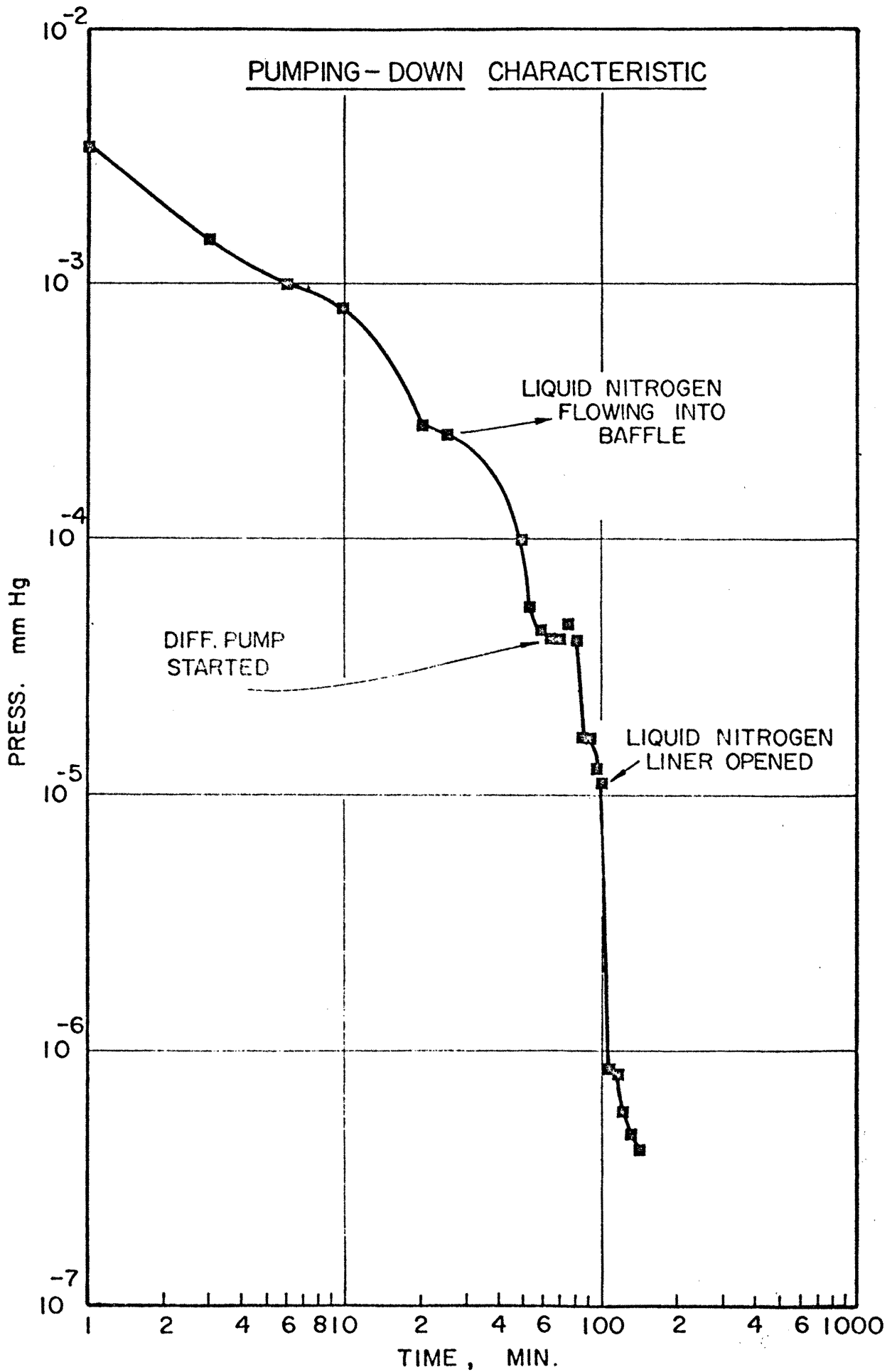


NOTES:
 1 - ONLY FOR THE 2KV P.S.
 2 - ONLY FOR THE 5KV P.S.

FLUID DYNAMICS AND DIFFUSION LABORATORY CSU FT. COLLINS		
PROJECT	CSU HIGH VACUUM FACILITY	PROJECT NO. 1509
TITLE HIGH VOLTAGE POWER SUPPLIES		
DESIGN BY	SCINTELLONICS, INC.	DRAWN BY
DATE	JUNE 1964	DATE
		SEPT. 1964
SCHEMATIC NO.		

HIGH VOLTAGE POWER SUPPLIES COMPONENTS

<u>Component</u>	<u>2 KV P.S.</u>	<u>5 KV P.S.</u>
C ₁	2 μ F	1.25 μ F
C ₂	2 μ F	1.25 μ F
R1	1.8 M Ω	9 M Ω
R2	0.444 Ω	1.11 Ω
R3	1 K Ω	3.3 K Ω
R4	270 Ω	680 Ω
R5	120 Ω	270 Ω
R6	68 Ω	150 Ω
R7	47 Ω	100 Ω
R8	33 Ω	68 Ω
R9	27 Ω	47 Ω
R10	18 Ω	39 Ω
R11	15 Ω	27 Ω
R12	128 Ω	265 Ω
R13	1 K Ω	200-1000 Ω
R14	0	17 K Ω
R15	42 K Ω	100 K Ω
R16	0	22 K Ω
R17	42 K Ω	100 K Ω
R18	0	22 K Ω
R19	42 K Ω	100 K Ω
R20	0	22 K Ω
R21	42 K Ω	100 K Ω
R22	0	22 K Ω
R23	42 K Ω	100 K Ω
R24	0	22 K Ω
R25	42 K Ω	100 K Ω
R26	0	22 K Ω
R27	42 K Ω	100 K Ω
R28	0	22 K Ω
R29	42 K Ω	100 K Ω
R30	0	22 K Ω
R31	42 K Ω	100 K Ω
R32	0	22 K Ω
R33	42 K Ω	100 K Ω



THESIS

SECONDARY EMISSION
EFFECTS IN ION BEAMS

Submitted by

Carlos A. Marazzi

In partial fulfillment of the requirements

for the Degree of Master of Science

Colorado State University

Fort Collins, Colorado

November, 1964

ABSTRACT OF THESIS

SECONDARY EMISSION EFFECTS IN ION BEAMS

There are many reasons to believe that electric propulsion is the most suitable way, known at the present time, of thrusting rockets for very long trips in space. In the last few years, many research works have been conducted on the explanation of phenomena occurring in, and the design of, electrostatic thrusters.

In one of these research works, it was found that the power of an ion-beam engine, when an electron source is introduced into it, increases remarkably in regard to the expected values. This could have been due to a meaningful space charge compensation of the ion beam by secondary emission. This research work attempts to verify this explanation of the phenomenon.

This thesis is based on existing publications that deal with the solution of ambipolar space-charge problems.

The result of the analytical treatment of the proposed model shows that the unexpected power increase could have hardly been due solely to the space-charge compensation.

Carlos Marazzi
Electrical Engineering Department
Colorado State University
November, 1964

ACKNOWLEDGEMENTS

The author wishes to express his appreciation to Professors Virgil A. Sandborn and R. John Morgan for their helpful guidance and counseling.

Sincere thanks are due to Drs. Lee M. Maxwell and Lionel V. Baldwin for their help in discussing various problems associated with this work.

This research was made possible by a grant of the National Aerospace Administration.

TABLE OF CONTENTS

	<u>Page</u>
INTRODUCTION	1
BACKGROUND OF THE PROBLEM	1
THE MECHANISM OF THE PHENOMENA	3
SPACE CHARGE DISTRIBUTION IN THE CASE TO BE CONSIDERED	3
POISSON'S EQUATION FOR TWO DIFFERENT SPACE CHARGES FLOWING IN THE SAME DIRECTION	7
EVALUATION OF J_p / J_{po}	12
CONCLUSION	16
ANNOTATED BIBLIOGRAPHY	18
SOURCES CONSULTED	19
APPENDIX	21

LIST OF FIGURES

<u>No.</u>	<u>Title</u>	<u>Page</u>
1	Proposed model with an ion-emitter and an electron-emitter.....	4
2	Simplified model	4
3	Current density increase in function of the dimensionless kinetic energy of the secondary electrons	15
4	Net of points for two infinite parallel plates.....	23
5	Flow-chart for program (I)	27
6	Potential field for $C = 10$	33
7	Potential distribution at the center of the system	34
8	Potential field for $C = 10$. Program (II)	42
9	Potential distribution. Program (II)	43
10	Value of $X(11, 10)$. Program (II).....	44
11	Rate of change of $X(11, 10)$. Program (II)	45
12	Potential field. Program (III).....	50
13	Potential distribution. Program (III)	51

LIST OF TABLES

<u>No.</u>	<u>Title</u>	<u>Page</u>
1	Current increase in ambipolar space charge.....	13
2	Poisson and Laplace equation in same space	30
3	Poisson and Laplace equation in same space with a disturbance, and zero initial velocity	37
4	Poisson and Laplace equation in same space with a disturbance, and finite initial velocity.....	46

INTRODUCTION

Sandborn and Baldwin [1]¹ found (during experimentations with a focused ion-beam-thruster) that the ion-beam-power increases remarkably by introducing, close to the ion-emitter, an electron-source. This increase in beam power is many times over the expected values.

The first part of this thesis gives an outline of thoughts developed during preliminary study of a possible model which might explain the increase of power in the ion-beam-thruster.

The second part deals with the analytical solution of a proposed model and the evaluation of special cases. The evaluation, using a digital computer, of the potential distribution between infinite parallel plates with space-charges and space-charge-free zones is given in an appendix.

BACKGROUND OF THE PROBLEM

An exact mathematical description of the current increase when two different "charge carriers" are flowing in the same space and in opposite directions is given in Ref. [2] and [3]. Paper [2] by I. Langmuir from the year 1929 describes: electric field, potential, and space-charge distributions.

¹ For bracketed references, see Annotated Bibliography on page 18.

Müller-Lübeck [3] makes a rigorously mathematical analysis using the same model as I. Langmuir. Both consider the ideal case of parallel plane surfaces for the electrodes and zero initial velocity of the "charge carriers". The electric field is zero at the surfaces. These works and others on the subject have concluded that current density increases of about 1.86 times, with respect to the case of the unipolar flow are possible. This density increase occurs when:

$$\frac{J_p}{J_e} \sqrt{\frac{m_p}{m_e}} = 1.0$$

where:

m_p and m_e are the masses of the ions and electrons;

J_p and J_e are the current densities;

that is, when both space charges are of equal number. However, the observed increase of current in the ion-beam-thruster [1], was up to 25 times greater than without the electron source.

In this case [1], the electron-source was a thoriated tungsten wire ring of 1.43 cm (0.57 inch) diameter heated to about 1370°K. The accelerating potentials used during the experimentation were from 2 to 5 kV, and the focusing used was a Pierce accelerator system. This focusing system assumes a very thin beam, so that in the aperture of the accelerator the potential surface should approximate a plane. In the case of the thruster, the aperture was 2.05 cm (0.83 inch), and the ratios $\frac{L}{D}$ (D stands for the diameter of the beam

and L for the distance between the accelerators) that were used, were between 0.6 and 1.4. These low values for $\frac{L}{D}$ cause the beam to spread, so that the potential surface in the accelerator's aperture is no longer a plane, and as a consequence the electric field is non-homogeneous. In [1] (Fig. 13 and 14) the amount of power lost by the non-homogeneity is shown.

THE MECHANISM OF THE PHENOMENA

There are various theories with respect to this phenomenon. One possible mechanism is that the electrons arriving to the ion-emitter with high energy produce a large number of secondary electrons. These secondary electrons should create a negative-space charge in the same place or near the ion's "virtual cathode". The potential and the field distributions will be modified, thus reducing the space charge and a greater number of ions can leave the ion's virtual cathode.

In the case here considered the bipolar space charge is created by two sources. One is an ion-emitter in an accelerating field. The other is the secondary emission of electrons produced by primary electrons with high energy coming from an electron-emitter.

SPACE CHARGE DISTRIBUTION IN THE CASE TO BE CONSIDERED

Figure 1 shows the system composed of an ion-emitter and an electron-emitter. The ions are emitted with an initial velocity

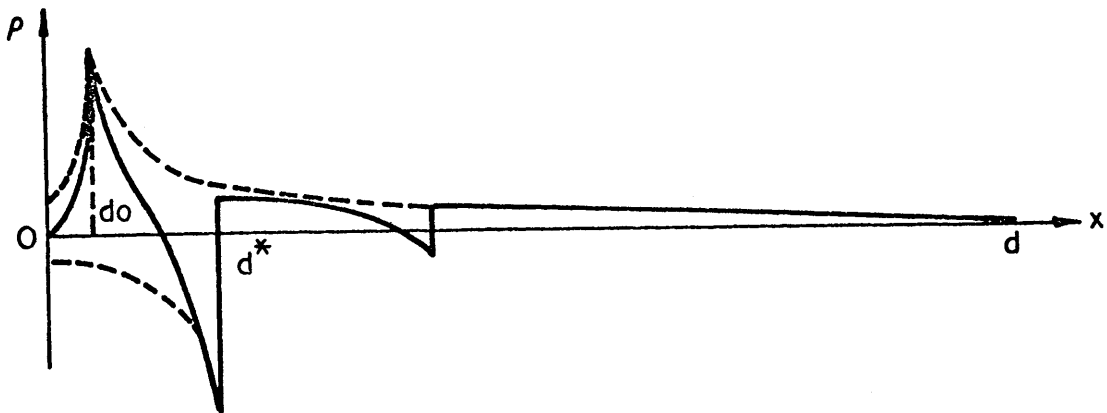
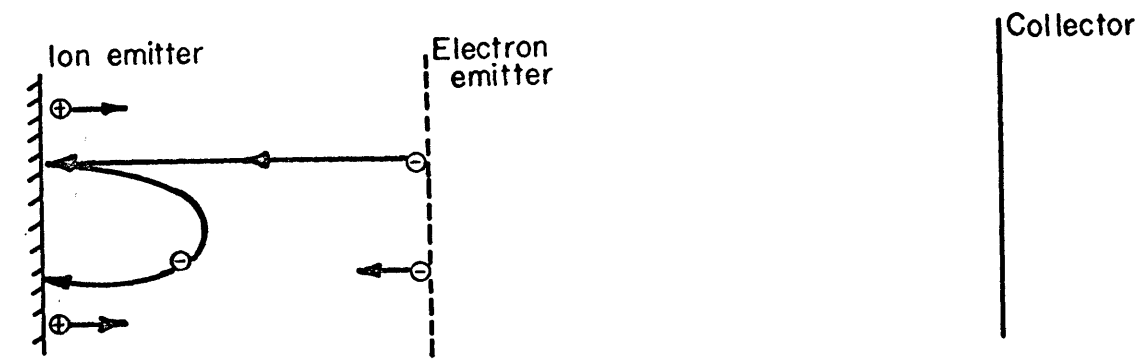


FIG. 1 PROPOSED MODEL WITH AN ION-EMITTER AND AN ELECTRON-EMITTER

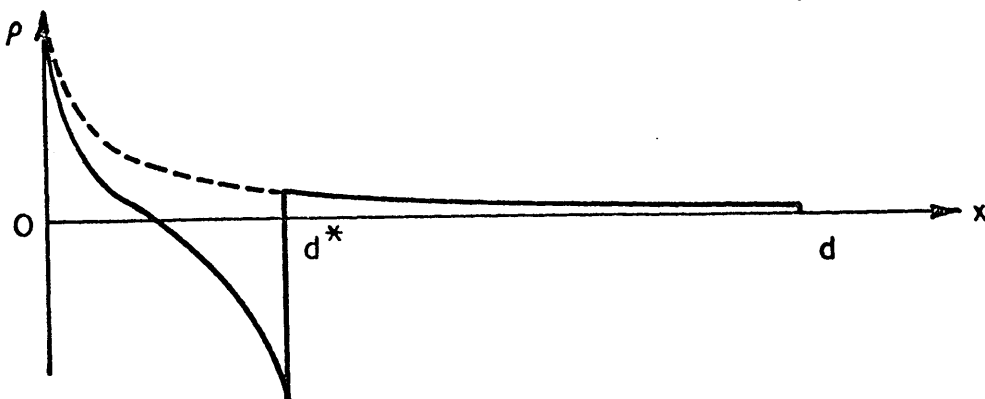
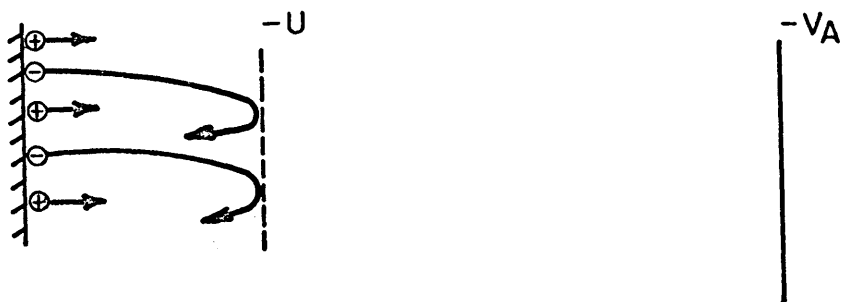


FIG. 2 SIMPLIFIED MODEL

$V_{po} \neq 0$ and create in the neighborhood of the emitter a cloud of positive charges. In this cloud the ions have zero uniform velocity and therefore the space charge has a maximum value.

The electrons are emitted also with an initial velocity $V_{eo} \neq 0$ and are accelerated in a high potential field, making a very small contribution to the space charge near the ion-emitter.

The electrons arriving at the ion-emitter with high energy produce secondary electrons with energies between 2 to 20 volts. These secondary electrons are in a retarding field and after losing their kinetic energy fall back to the ion-emitter and probably cause tertiary electrons. In this way a negative space charge is created near the emitter which reduces the space charge-limitation of the ions. Figure 1 shows also the approximate space charge distribution.

To study the problem of the ion current increase due to the effect of the negative space-charges only the space between d_0 and d^* is considered. This is done because the space between $x = 0$ and $x = d_0$ is influenced mainly by the ions space charge, where the ions have velocities between the thermal initial velocity V_{po} and zero at d_0 . The space between d^* and d is mainly influenced by the accelerating ions and the secondary electrons. Because the primary electron source will give a secondary contribution only and may not be parallel to the ion beam, it is not considered in the study of ion current increase. The result of these simplifications is the model

shown in Figure 2. The secondary electron-space charge has a finite value at the surface of the emitter given by the initial velocities of the electrons, and it increases in almost hyperbolic form until the point d^* . At d^* the electrons lose their kinetic energy and the space charge reaches a maximum. Therefore, with regard to the space charge effects, the electron current going from the emitter to d^* , and the one coming back to the emitter, can be considered as twice the current flowing from d^* to the emitter. The electrons have zero initial velocity at d^* and a finite velocity V_{e0} at the emitter.

For the space between $x = 0$ and $x = d^*$, the problem is similar to the one explained in [2] and [3]. The main differences are: the distance between "plates" is not constant and a decrease of the distance can give a further increase of the current; and the ratio of space charges is a function of the primary electron current, which can be controlled by the temperature of the electron emitter.

The location where the electrons have zero velocity and turn back to the emitter will always be beyond the main positive space charge region, because as long as the electrons are moving in the positive space charge they do not see a meaningful retarding potential. There is no possibility that the maximum of the negative charge can be at the same location as the positive charge. However, there must be a location where the negative space charge has a maximum, because there is a location where the electrons have zero velocity and

fall back to the emitter. Thus a partial "neutralization" of the positive space charge takes place.

Assuming the absence of electrons and zero initial velocity for the ions, the ion current density [5] is given by

$$J_{po} = \frac{4}{9} \epsilon_o \sqrt{\frac{2e}{m_p}} \frac{V_A^{3/2}}{d^2} \quad (1)$$

where J_{po} = ion current density in A/cm²;

d = distance between emitter and point where the potential is V_A ;

e = charge of each ion. (It is considered of the same absolute value as the charge of an electron, because it is assumed that there is single ionization only.)

POISSON'S EQUATION FOR TWO DIFFERENT SPACE CHARGES FLOWING IN THE SAME DIRECTION

To find the ion current increase due to presence of secondary electrons at the ion-emitter's surface, we solve the Poisson's equation for the simplified model explained above.

Here we make use again of Figure 2. In this case the ions are in an accelerating field and the electrons in a retarding field. Thus the energy equations are

$$\frac{1}{2} m_p v_p^2 = eV \quad (2)$$

$$\frac{1}{2} m_e v_e^2 = \frac{1}{2} m_e v_{eo}^2 - eV \quad (3)$$

which gives
$$v_p = \sqrt{\frac{2e}{m_p}} \sqrt{V} \quad (4)$$

and
$$v_e = \sqrt{v_{eo}^2 - \frac{2e}{m_e} V} \quad (5)$$

The general expression of Poisson's equation is:

$$\frac{d^2V}{dx^2} + \frac{1}{\epsilon_0} \sum \rho = 0 \quad (6)$$

$$\sum \rho = \rho_p - \rho_e \quad (7)$$

$$\frac{d^2V}{dx^2} = \frac{1}{\epsilon_0} (\rho_e - \rho_p) \quad (8)$$

and in terms of the current densities and velocities

$$\frac{d^2V}{dx^2} = \frac{1}{\epsilon_0} \left(\frac{J_p}{v_p} - \frac{J_e}{v_e} \right) \quad (9)$$

$$\frac{d^2V}{dx^2} = \frac{1}{\epsilon_0} \left[J_p \sqrt{\frac{m_p}{2e}} \frac{1}{\sqrt{V}} - J_e \sqrt{\frac{m_e}{2e}} \frac{1}{\sqrt{v_{eo}^2 - \frac{m_e}{2e} V}} \right] \quad (10)$$

defining:
$$U^* = v_{eo}^2 \frac{m_e}{2e} \quad (11)$$

$$a = \frac{J_p}{J_e} \sqrt{\frac{m_p}{m_e}} \quad (12)$$

substituting into equation (10):

$$y = \frac{V}{V_A} ; y^* = \frac{U^*}{V_A} \quad (13)$$

$$s = \frac{x}{d} ; s^* = \frac{d^*}{d}$$

and using equation (1), we find:

$$\frac{d^2y}{ds^2} = \frac{4}{9} \frac{J_p}{J_{po}} \left[\frac{1}{\sqrt{y}} - \frac{1}{a} \frac{1}{\sqrt{y^* - y}} \right] \quad (14)$$

For the space between $x = 0$ and $x = d^*$, integrating according to:

$$\frac{1}{2} \frac{d}{ds} \left[\left(\frac{dy}{ds} \right)^2 \right] = \frac{dy}{ds} \frac{d^2y}{ds^2} \quad (15)$$

we integrate twice as follows:

$$\left(\frac{dy}{ds} \right)^2 = \frac{8}{9} \frac{J_p}{J_{po}} \int_0^y \left(\frac{1}{\sqrt{y}} - \frac{1}{\sqrt{y^* - y}} \right) dy \quad (16)$$

to integrate with limits between 0 and 1 we change the variable

$$\mu = \frac{y}{y^*} ; \quad (17)$$

and thus:

$$\frac{d\mu}{ds} = \frac{4}{3} y^{*-3/4} \sqrt{\frac{J_p}{J_{po}}} \left[\sqrt{\mu} + \frac{1}{a} \left(\sqrt{1 - \mu} - 1 \right) \right]^{1/2} \quad (18)$$

Integrating again:

$$\int_0^{s^*} ds = \frac{3}{4} y^{*3/4} \sqrt{\frac{J_{po}}{J_p}} \int_0^1 \frac{d\mu}{\left[\sqrt{\mu} + \frac{1}{a} \left(\sqrt{1 - \mu} - 1 \right) \right]^{1/2}} \quad (19)$$

$$s^* = y^{*3/4} \sqrt{\frac{J_{po}}{J_p}} h \left(\mu, \frac{1}{a} \right) \quad (20)$$

where $h(\mu, \frac{1}{a})$ is $\frac{3}{4}$ of the right side integral. This integral was solved for a similar case in [3].

Solving now for the space between d^* and d , ($a = \infty$), equation (14)

becomes:

$$\frac{d^2y}{ds^2} = \frac{4}{9} \frac{J_p}{J_{po}} \frac{1}{\sqrt{y}} \quad (21)$$

The first integration gives

$$\left(\frac{dy}{ds}\right)^2 = \frac{8}{9} \frac{J_p}{J_{po}} 2y^{1/2} + C \quad (22)$$

The evaluation of C can be obtained from equation (16) after integrating for $s = s^*$, that is:

$$\left(\frac{dy}{ds}\right)^2 \Big|_{s=s^*} = \frac{16}{9} \frac{J_p}{J_{po}} y^{*1/2} \left(1 - \frac{1}{a}\right) \quad (23)$$

$$C = -2y^{*1/2} \frac{1}{a} \frac{8}{9} \frac{J_p}{J_{po}} \quad (24)$$

Substituting in equation (22) and integrating again:

$$\int_{s^*}^1 ds = \frac{3}{4} \left(\frac{J_{po}}{J_p}\right)^{1/2} \int_{y^*}^1 \frac{dy}{\left[y^{1/2} - \frac{1}{a} y^{*1/2}\right]^{1/2}} \quad (25)$$

$$1 - s^* = \left(\frac{J_{po}}{J_p}\right)^{1/2} R\left(y^*, \frac{1}{a}\right) \quad (26)$$

where $R\left(y^*, \frac{1}{a}\right)$ can be solved substituting: $y = t^2$.

$$R\left(y^*, \frac{1}{a}\right) = \frac{3}{4} 2 \int_{\sqrt{y^*}}^1 \frac{t dt}{\sqrt{t - \frac{1}{a}} \sqrt{y^*}} \quad (27)$$

$$R\left(y^*, \frac{1}{a}\right) = \left(\frac{2}{a}\sqrt{y^*} + 1\right) \sqrt{1 - \frac{1}{a}\sqrt{y^*}} - y^{*3/4} \left(1 + \frac{2}{a}\right) \sqrt{1 - \frac{1}{a}} \quad (28)$$

Solving for the case $a = 1$, the expression for $R(y^*, 1)$ becomes

$$R(y^*, 1) = (2\sqrt{y^*} + 1) \sqrt{1 - \sqrt{y^*}} \quad (29)$$

$a = 1$, stands for equal amount of space charges in the space between $x = 0$ and $x = d^*$. For the case of cesium atoms the value of $\sqrt{\frac{m_p}{m_e}}$ is about 500 (see footnote 2).

Therefore, an electron current density 500 times the ion current density, is necessary to approach the value $a = 1$. Thus, we have two equations, (20) and (26) with the unknown s^* . Substituting equation (20) in (26) we obtain:

$$\frac{J_p}{J_{po}} = \left(y^* \frac{3}{4} h\left(\mu; \frac{1}{a}\right) + R\left(y^*, \frac{1}{a}\right) \right)^2 \quad (30)$$

The value of $h(1, 1)$ was evaluated in [2] and [3] and is 1.36134.

Equation (30) becomes:

$$\frac{J_p}{J_{po}} = \left[1.36134 y^* \frac{3}{4} + R(y^*, 1) \right]^2 \quad (31)$$

² Electron mass: $m_e = 9.11 \times 10^{-28} \text{ g}$

Cs - ion mass: $m_p = (Z + N)1837 m_e$

$$\sqrt{\frac{m_p}{m_e}} = \sqrt{244,321}$$

$$a = 494.28 \frac{J_p}{J_e}$$

EVALUATION OF J_p/J_{po}

The function $(J_p/J_{po}) = f(y^*)$ was evaluated for the case of $a = 1$. This case represents a very large electron space-charge.

Table I shows the program and the results obtained.

Figure 3 shows that the current density increase as a function of the dimensionless kinetic energy of the secondary electrons, $y^* = U^*/V_A$. A maximal current increase of 4.5725 is obtained when the secondary electrons have a kinetic energy of 0.60 with respect to the applied acceleration potential.

TABLE I

SOURCE PROGRAM

C CURRENT INCREASE IN AMBIPOLAR SPACE CHARGE

```
      Y = 0.0
      X = Y-1.0
11  IF (X) 1, 1, 2
      1  D = (1.36134*SQRTF(SQRTF(Y**3)) + (2.*SQRTF(Y) + 1.)*SQRTF(1.-SQRTF(Y)))**2
10  FORMAT (2F10.6)
      PRINT 10, Y, D
      PUNCH 10, Y, D
      Y = Y + 0.05
      GO TO 11
2  END
```

TABLE I (cont'd)

RESULT

y^*	J_p / J_{po}
0.000000	1.000000
.050000	2.013929
.100000	2.534369
.150000	2.948747
.200000	3.296529
.250000	3.592995
.300000	3.845727
.350000	4.058865
.400000	4.234664
.450000	4.374175
.500000	4.477542
.550000	4.544128
.600000	4.572500
.650000	4.560294
.700000	4.503924
.750000	4.398000
.800000	4.234159
.850000	3.998455
.900000	3.664365
.950000	3.165833
1.000000	1.853246

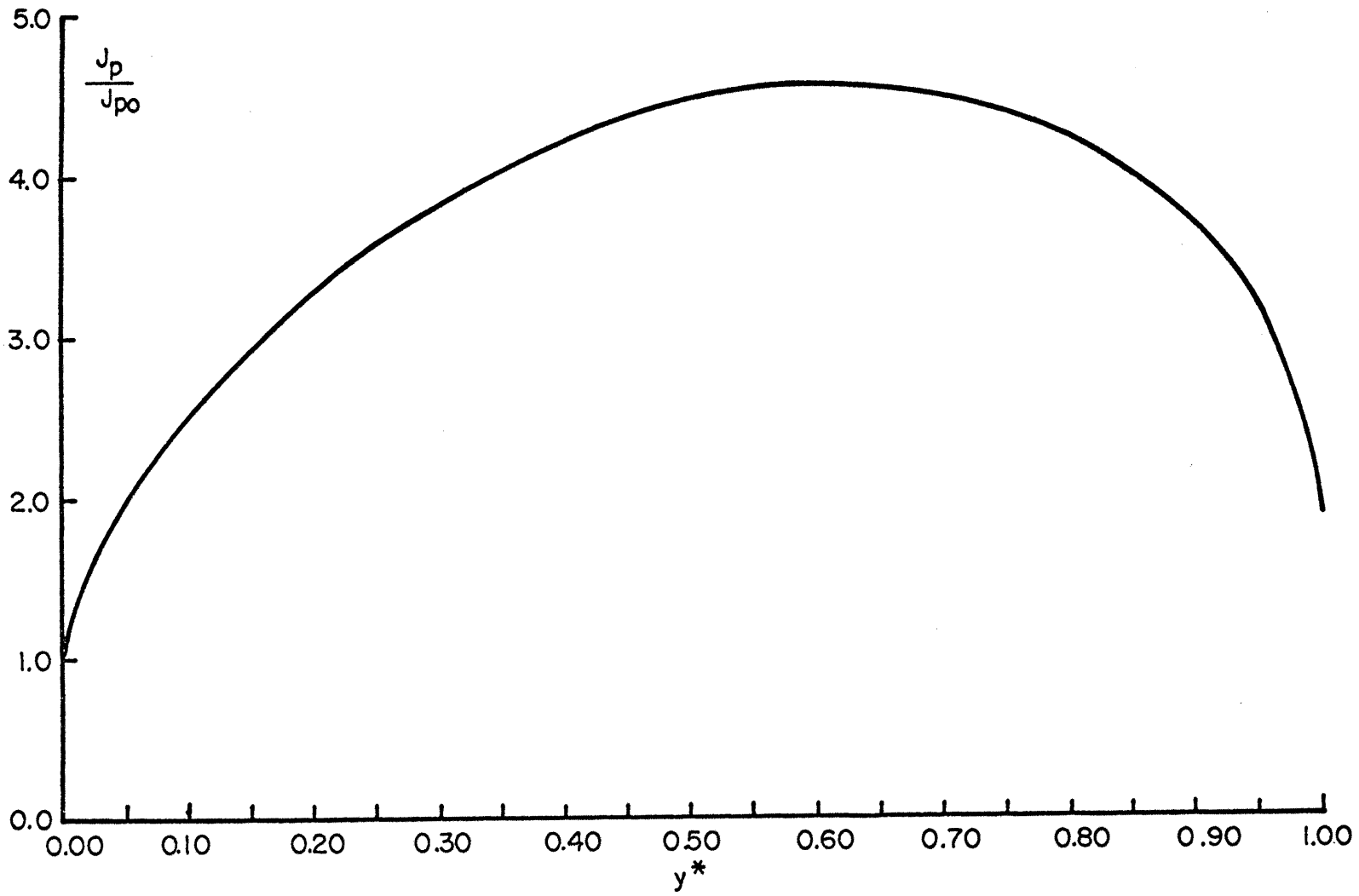


FIG. 3 CURRENT DENSITY INCREASE IN FUNCTION OF THE DIMENSIONLESS KINETIC ENERGY OF THE SECONDARY ELECTRONS

CONCLUSION

The problem considered herein differs from that considered by Langmuir [2] in two respects: first, there is as many electrons as ions present, while Langmuir is considering an electron rich system only; second, the present analysis is concerned with the acceleration of ions rather than electrons.

From the model adopted for this analysis, and its evaluation, it seems improbable that the large amount of power observed at the output of the ion beam-thruster [1] is due only to the effect of space charge compensation by the secondary emission.

It is possible that the observed phenomena could have been helped by a second production of ions in the space between the ion-emitter and the accelerator system. This, of course, could only happen if enough molecular cesium flows out of the cesium boiler without being ionized while crossing the porous tungsten. If this was the case, the large current increase might have been due to collision ionization of the free cesium molecules by the primary electrons. The electrons were emitted in a high accelerating potential field, sufficient to ionize the neutral cesium.

Another supporting argument for this assumption is the impingement effect observed (see Fig. 13 in [1]). The impingement of the outside ions of the beam with the accelerator's edge could cause secondary emission. These secondary electrons find a high

potential accelerating field toward the ion-emitter and thus possibly collide with neutral cesium atoms in their trajectory to the ion-emitter. Because that can occur in any place inside of the accelerator system, the ionized atoms are not forced to cross the space charge limitation zone resulting in a further increase of ions current.

Recently, a paper by Walton L. Howes (Lewis Research Center, Cleveland, Ohio, NASA Technical Note, NASA TN D-2425, of August, 1964, was published showing that the current increase in a space with ambipolar charges can be 25 times greater, if the initial kinetic energy of the charges is about 5 times its potential energy. Since these initial conditions appear inconsistent with the observed phenomenon no consideration was given to it.

ANNOTATED BIBLIOGRAPHY

- [1] Baldwin, L. V. and V. A. Sandborn, Hot-Wire Calorimeter Study of Ion Production and Acceleration. AIAA Journal, Volume 2, Number 4. April, 1964. pp. 660-666.
- [2] Langmuir, Irving. The Interaction of Electron and Positive Ion Space Charges in Cathode Sheets. Physical Review 33, Number 6, June, 1929. pp. 954-989.
- [3] Müller-Lübeck, K., Über die ambipolare Raumladungsströmung bei ebenen Elektroden. Zeitschrift für Angewandte Physik, Volume 3, Number 11, 1951. pp. 409-415.
- [4] Rothe, H. and Werner Klenn, Grundlagen und Kennlinien der Elektronenröhren. Leipzig. Akademische Verlagsgesellschaft, 1948.
- [5] Spanenberg, K. R., Vacuum Tubes. New York: McGraw-Hill, 1948.
- [6] Kunz, Kaiser S., Numerical Analysis. New York: McGraw-Hill, 1957.
- [7] Grabbe, E. M., S. Ramo and D. E. Worldridge, Handbook of Automation, Computation and Control. Volume 1; New York: J. Wiley and Sons, 1958.

SOURCES CONSULTED:

1. Azaroff, L. V. and J. J. Brophy, Electronic Processes in Materials. New York: McGraw-Hill, 1963.
2. Baldwin, L. V. and V. A. Sandborn, Hot-Wire Calorimeter Study of Ion Production and Acceleration. AIAA Journal, Volume 2, Number 4, April, 1964. pp. 660-666.
3. Bruining, H., Physics and Applications of Secondary Electron Emission. New York: McGraw-Hill, 1954.
4. Campbell, William G., A Form Book for Thesis Writing. New York: Houghton Mifflin Company, 1939.
5. Grabbe, E. M., S. Ramo and D. E. Worldridge, Handbook of Automation, Computation and Control. 3 volumes; New York: J. Wiley and Sons, 1958.
6. Hamza, V. and E. Richley, Numerical Solution of Two-Dimensional Poisson Equation: Theory and Application to Electrostatic Ion-Engine Analysis. NASA Technical Note E-1323, October, 1962.
7. _____, Numerical Evaluation of Ion-Thruster Optics. NASA Technical Note D-1665, May, 1963.
8. Jahnke, E. and F. Emde, Tables of Functions with Formulae and Curves. Fourth edition; New York: Dover Publications, 1945.
9. Jonker, J. L. H., On the Theory of Secondary Electron Emission. Philips Research Reports 7, 1-20, February, 1952.
10. Kunz, Kaiser S., Numerical Analysis. New York: McGraw-Hill, 1957.
11. Kuskevics, G., Criteria and a Graphical Method for Optimization of Cesium Surface Ionizer Materials. Electro-Optical-System, Inc., Pasadena, California; Research Report No.3, January, 1962.
12. Langmuir, Irving. The Interaction of Electron and Positive Ion Space Charges in Cathode Sheets. Physical Review 33, No.6, June, 1929, pp. 954-989.

SOURCES CONSULTED cont'd:

13. Langmuir, D. B., E. Stuhlinger and J. M. Sellen, Jr., Electrostatic Propulsion. 5 volumes; New York: Academic Press, 1961.
14. Lockwood, D. L., and V. Hamza, Space-charge-flow Theory and Electrode Design for Electrostatic Rocket Engines. NASA Technical Note D-1461, December, 1962.
15. Müller-Lübeck, K., Über die ambipolare Raumladungsströmung bei ebenen Elektroden. Zeitschrift für Angewandte Physik, volume 3, number 11, 1951, pp. 409-415.
16. Richley, E. and W. R. Mickelsen, Effects of Molecular Flow in Plasma Generation and some Analyses of Space Charge Flow in Ion Acceleration. NASA Technical Preprint 21-63, January 1964.
17. Rint, C., Handbuch für Hochfrequenz und Elektrotechnik. 6 Bände; Berlin. Verlag für Radio-Foto Kinotechnik GmbH. 1952.
18. Rothe, H. and Werner Klenn, Grundlagen und Kennlinien der Elektronenröhren. Leipzig. Akademische Verlagsgesellschaft, 1948.
19. Spanenberg, K. R., Vacuum Tubes. New York: McGraw-Hill, 1948.
20. _____, Fundamentals of Electron Devices. New York: McGraw-Hill, 1957.
21. Taylor, J. B. and I. Langmuir, The Evaporation of Atoms, Ions, and Electrons from Caesium Films on Tungsten. Physical Review 44, 1933, pp. 423.
22. Zworykin, V. K. and G. A. Morton, Television. Second edition; New York: J. Wiley and Sons, 1954.

APPENDIX

METHODS FOR CALCULATING ELECTRIC FIELDS CONTAINING
SPACE-CHARGE AND SPACE-CHARGE-FREE ZONES

To obtain the potential distribution in a space-charge field between two infinite parallel plates it is necessary to solve Poisson's equation in only one dimension [4]:

$$\frac{d^2U}{dx^2} = - \frac{\rho_i}{\epsilon_0} \quad (1)$$

ρ_i is a function of U , such that

$$\frac{d^2U}{dx^2} = - C_1 \sqrt{U} \quad (2)$$

where C_1 is a constant for a given case.

The use of a digital computer simplifies considerably the work necessary to find the potential distribution, and increases the accuracy. This problem was solved with a digital computer, IBM 1620, using the language Fortran II. Figure 4 shows two parallel plates containing space-charge and space-charge-free zones. The two horizontal lines represent the parallel plates. It is assumed that they are infinite to the left and to the right. An ion beam goes from the zero potential plate to the -100 volt plate, only at the center of the system. Thus, in this area ρ_i will be different from zero [4]. Equation (3) gives the function of ρ_i

$$\rho_i = J \sqrt{\frac{m}{2e}} \cdot \sqrt{\frac{1}{U}} \quad (3)$$

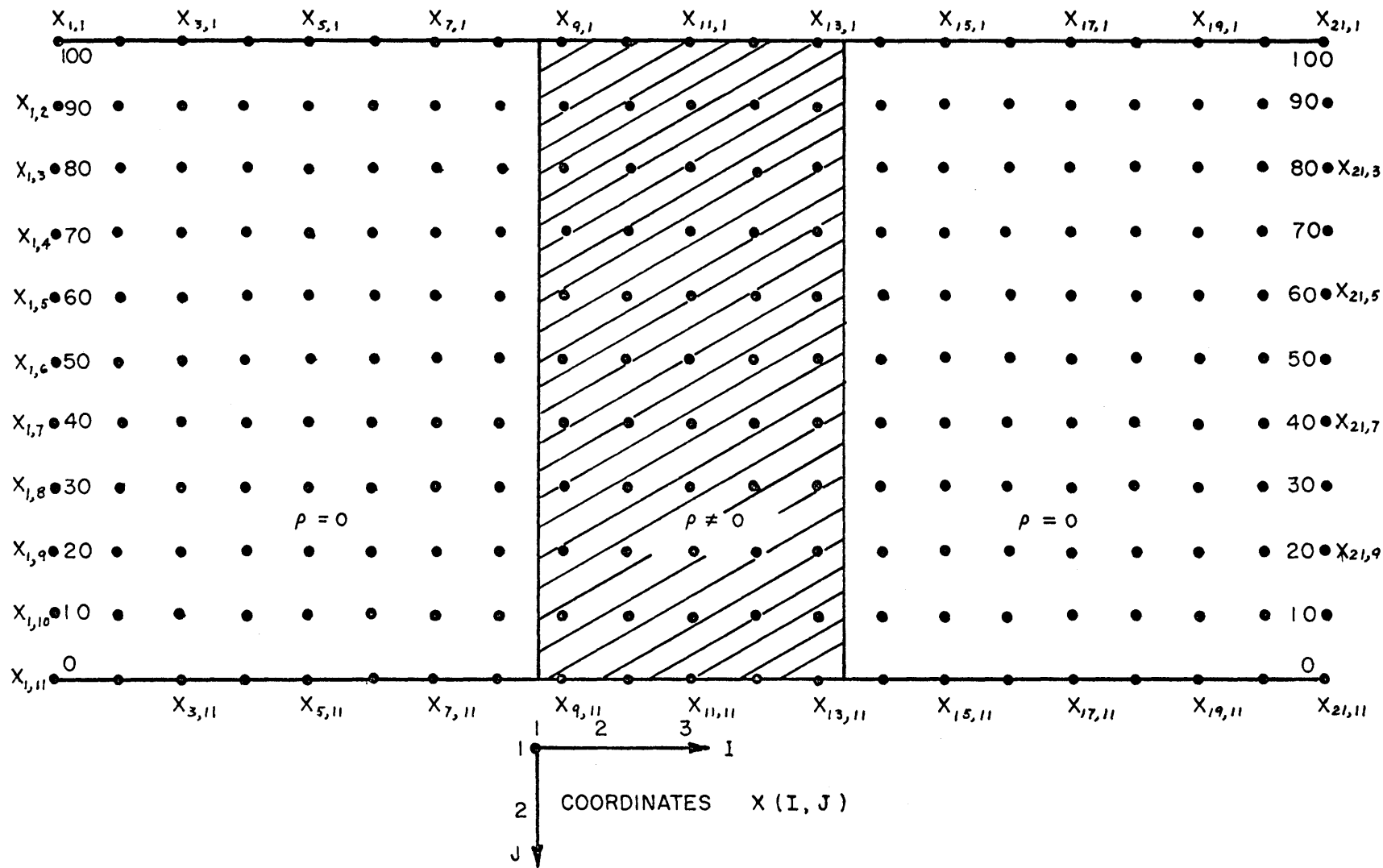


FIG. 4 NET OF POINTS FOR TWO INFINE PARALLEL

where: J is the current density, m is the ion mass, and e is the ions charge. On the left and right side of the beam, ρ_i is equal to zero.

An iterative method was used to calculate the potential lines. The function to be computed is equation (4). It is termed the Liebmann improvement formula of Poisson's equation ([6] page 317 and 318).

The field is defined by a net of points as shown in Figure 4. Each of the points is a location in the program, and the values of the points are their corresponding potentials. By averaging the four adjacent potentials as shown in equation (4):

$$U_{i,j} = \frac{U_{(i-1,j)} + U_{(i+1,j)} + U_{(i,j-1)} + U_{(i,j+1)} - \rho_i \epsilon_0}{4} \quad (4)$$

the new value will be obtained for the point under consideration. The subindices i in equation (4) refer to the columns of points in the net of Figure 4. The subindices j refer to the rows.

At infinity in both directions, left and right, the potential gradient is constant. To simulate this situation, fixed potentials will be assigned with a constant gradient to the left-most and right-most column of the net. This is only an approximation, because the constant gradient is very far from the space-charge zone. The error of this approximation can be reduced by setting the constant gradient farther from the space-charge zone as in the case of Figure 4. The iterative method used here is fully justified as follows:

Poisson's equation for a two dimensional field is

$$\frac{\partial^2 U}{\partial z^2} + \frac{\partial^2 U}{\partial y^2} = \frac{-\rho}{\epsilon_0} \quad (15)$$

Using increments for the first derivative, it will be obtained ([6], [7]):

$$\frac{\partial U}{\partial z} = \frac{U(z + \Delta z, y) - U(z, y)}{\Delta z}$$

for the second derivative:

$$\frac{\partial^2 U}{\partial z^2} = \frac{U(z + 2\Delta z, y) - U(z + \Delta z, y) - U(z + \Delta z, y) + U(z, y)}{(\Delta z)^2}$$

or:

$$\frac{\partial^2 U}{\partial z^2} = \frac{U(z + \Delta z, y) - 2U(z, y) + U(z - \Delta z, y)}{(\Delta z)^2}$$

and hence:

$$\frac{\partial^2 U}{\partial y^2} = \frac{U(z, y + \Delta y) - 2U(z, y) + U(z, y - \Delta y)}{(\Delta y)^2}$$

By taking the increments $|\Delta z| = |\Delta y| = \frac{1}{p}$, substituting in

equation (15) and calling $z = i$, and $y = j$, the following is obtained:

$$U(i + 1, j) + U(i - 1, j) + U(i, j - 1) + U(i, j + 1) - 4U(i, j) = \frac{-\rho}{\epsilon_0} \frac{1}{p^2}$$

This equation can be written in the form of equation (4) with only the difference of $1/p^2$. This factor affects the accuracy of the method.

In the case of a net formed by 10 x 10 points:

$$\frac{1}{p^2} = \frac{1}{100} .$$

Equation (4) is used here to obtain a field described by equation (1).

This is the case where a space charge is created by an emission,

and the potential function follows a "4/3 power law" given by

equation (5).

$$U_x = U_o \left(\frac{x}{d} \right)^{4/3} \quad (5)$$

It is assumed in equations (1) and (5) that the initial velocity of the ions is zero, however this is not the real case.

(I) THE PROGRAM

Table II shows the source program, the data, and the results of the processing of the condensed program.

Figure 5 shows the flow chart used for this program. The program starts by setting the boundary values of 100 for the upper plate, zero for the lower, and the constant gradient values at all places. This is the case of Laplace's equation. The accelerating potential for ions is negative and the upper plate should be -100, but this change of sign can be made in the results. The arithmetic operation to be evaluated is given by equation (4). Prior to calculating any potential $U_{i,j}$ (in the program called X(I,J)), the program has two decision-statements in order to set ρ_i equal to, or different from, zero. For the central columns, between column 9 and 13, ρ_i is made different from zero. The iterative approximations are made 20 times, and the results are punched in cards. Each card will contain half a row. The complete row will not be punched because the expected field lines are completely symmetrical with respect to the central line. A typing statement for X(11, 6) equivalent to the center

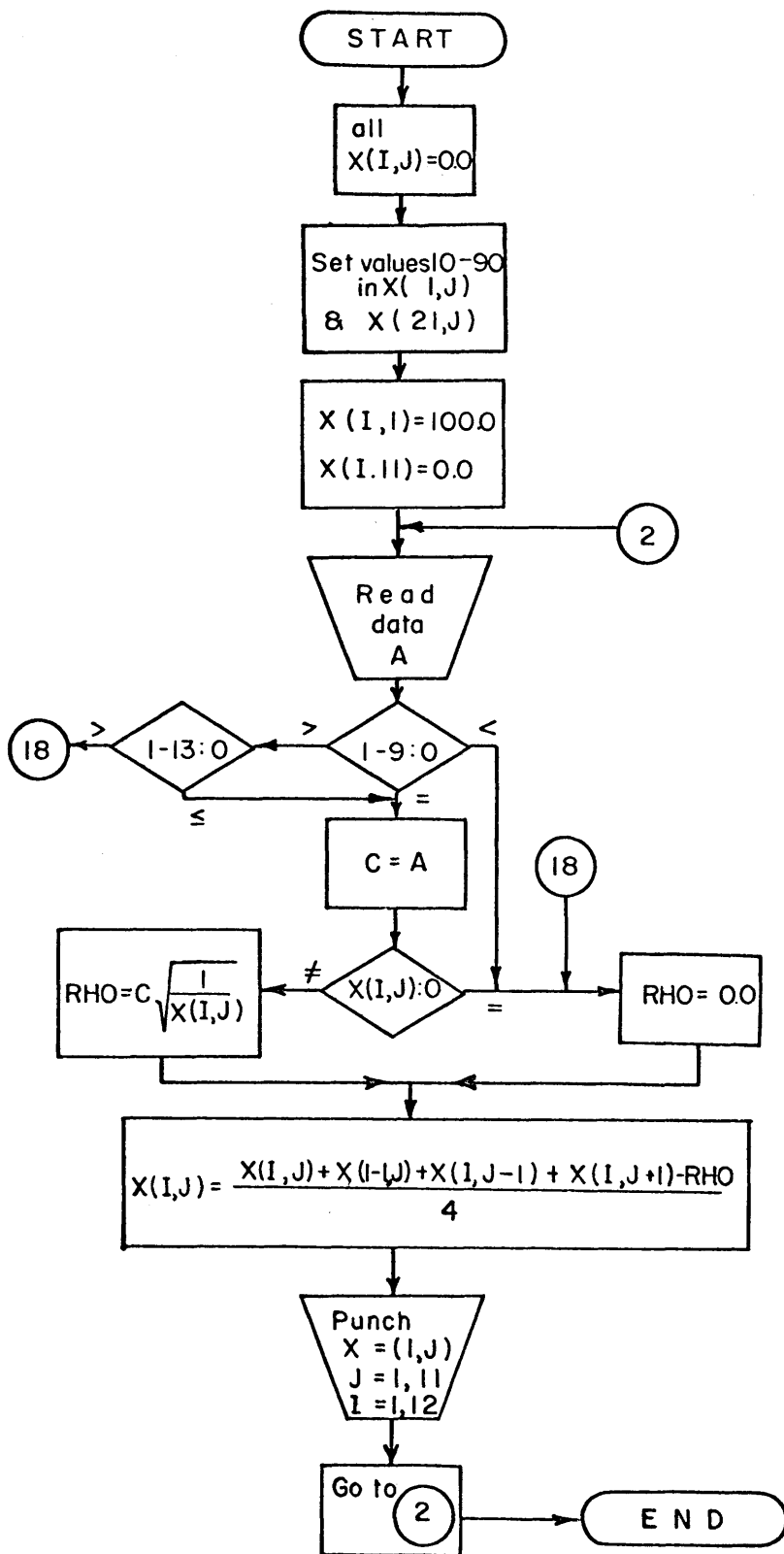


FIG. 5 FLOW-CHART FOR PROGRAM (1)

of the system, makes visible, after each iteration, the change from the previously calculated value, and therefore, the reduction of error. The same program and configuration can be used for an ion beam or an electron beam. The distinction can be made in the evaluation of the data obtained from the computer.

The processed equation is:

$$X_{(I, J)} = \frac{X_{(I-1, J)} + X_{(I+1, J)} + X_{(I, J-1)} + X_{(I, J+1)} - \text{RHO}}{4} \quad (5)$$

and

$$\text{RHO} = C \sqrt{\frac{1}{X_{(I, J)}}} \quad (6)$$

but to satisfy Poisson's equation, it must be:

$$\text{RHO} = \frac{\rho}{\epsilon_0} \frac{1}{p_1 p_2} \quad (7)$$

where p_1 and p_2 are the dimensions of the net. In this case

$$\frac{1}{p_1 p_2} = \frac{1}{200} . \text{ Considering equations (3), (6) and (7),}$$

$$C = \frac{1}{200} \frac{J}{\epsilon_0} \sqrt{\frac{m_e}{2e}} , \text{ where} \quad (8)$$

$\epsilon_0 = 8.86 \times 10^{-14} \left[\text{V}^{-1} \text{ A sec cm}^{-1} \right]$. For the case of an electron beam

$$\sqrt{\frac{m_e}{2e}} \approx 1.683 \times 10^{-8} \left[\text{V}^{1/2} \text{ sec cm}^{-1} \right] \quad (9)$$

Hence,

$$\frac{1}{\epsilon_0} \sqrt{\frac{m_e}{2e}} = 1.9 \times 10^5 \left[V^{3/2} A^{-1} \right]$$

and so:

$$C \approx J \times 10^3 .$$

Thus, if we enter with the data card the value of 10^{-3} , it will be read and located in A. When $\rho \neq 0$, C will be 10^{-3} and that corresponds to a current density of $J = 1 \text{ A/cm}^2$. Correspondingly, a current density of $J = 10 \text{ mA/cm}^2$, will be represented by a data card with the value of 10.

In the case of an ion-beam these numbers are different.

Equation (9) for cesium atoms will have the value of:

$$\frac{1}{\epsilon_0} \sqrt{\frac{m_i}{2e}} = 0.806 \times 10^8 \left[\frac{V^{3/2}}{A} \right]$$

Thus,

$$C = \frac{10^8}{200} \times J_i = 5 \times 10^5 \times J_i$$

This result shows that the ion current is 500 times less than an electron current for the same potential distribution. Figure 6 shows the obtained field lines, and Figure 7 shows the potential distribution of the center of the system.

This case corresponds to an electron current density of: 10 mA/cm^2 and an ion current density of: $20 \mu\text{A/cm}^2$.

This is the case of a space-charge between electrodes with zero electric field close to the emission surface. That means, that

(cont'd page 35)

TABLE II

C POISSON AND LAPLACE EQUATION IN SAME SPACE, PARALLEL PLATES,

```
DIMENSION X(21,11)
DO 1 I = 1,21
X(I,1) = 100.0
X(I,2) = 90.0
X(I,3) = 80.0
X(I,4) = 70.0
X(I,5) = 60.0
X(I,6) = 50.0
X(I,7) = 40.0
X(I,8) = 30.0
X(I,9) = 20.0
X(I,10) = 10.0
1 X(I,11) = 0.0
10 FORMAT (F6.3)
2 READ 10,A
DO 11 L = 1,20
3 FORMAT (F8.1)
PRINT 3, X(11,6)
DO 11 J = 2,10
DO 11 I = 2,20
IF (I-9) 18,5,6
5 C = A
GO TO 9
6 IF (I-13) 5,5,18
18 RHO = 0.0
```

continued next page

TABLE II (cont'd)

```
GO TO 11
9  RHO = C*SQRTF (1.00/x(I,J))
11 X(I,J) = (X(I-1,J) + X(I+1,J) + X(I,J-1) + X(I,J+1) - RHO) /4.0
DO 13 J = 1,11
12 FORMAT (12F6.1)
13 PUNCH 12,X(1,J),X(2,J),X(3,J),X(4,J),X(5,J),X(6,J),X(7,J),X(8,J)
1  X(9,J),X(10,J),X(11,J),X(12,J)
14 GO TO 2
END
```

TABLE II (cont'd)

POISSON EQUATION FOR $C = 10$

I:	1	2	3	4	5	6	7	8	9	10	11	12
	100.0	100.0	100.0	100.0	100.0	100.0	100.0	100.0	100.0	100.0	100.0	100.0
	90.0	89.9	89.9	89.9	89.7	89.5	89.2	88.7	87.9	87.5	87.3	87.4
	80.0	79.9	79.8	79.7	79.5	79.1	78.6	77.7	76.4	75.6	75.4	75.5
	70.0	69.9	69.8	69.6	69.3	68.8	68.0	66.8	65.2	64.2	63.8	64.1
	60.0	59.9	59.7	59.5	59.1	58.5	57.5	56.1	54.2	53.0	52.6	52.8
	50.0	49.9	49.7	49.4	49.0	48.3	47.2	45.6	43.4	42.1	41.5	41.9
	40.0	39.8	39.7	39.4	38.9	38.2	37.0	35.3	32.8	31.4	30.8	31.2
	30.0	29.9	29.7	29.4	29.0	28.3	27.1	25.3	22.7	21.1	20.5	20.9
	20.0	19.9	19.7	19.5	19.2	18.6	17.6	15.9	13.2	11.6	11.0	11.4
	10.0	9.9	9.8	9.7	9.5	9.2	8.5	7.4	5.0	3.7	3.2	3.6
	0.0	0.0	0.0	0.0	0.0	0.0	0.0	0.0	0.0	0.0	0.0	0.0

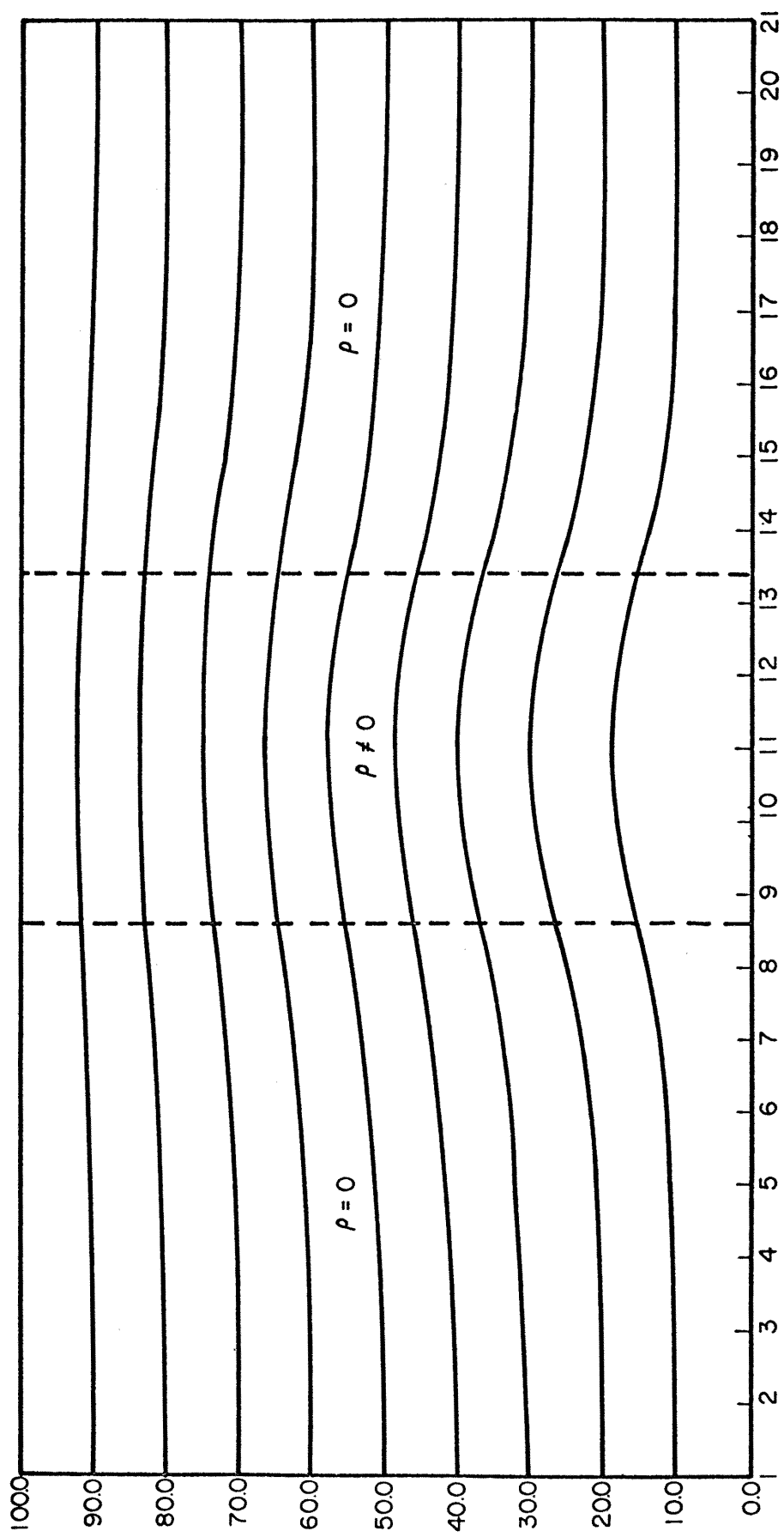


FIG.6 POTENTIAL FIELD FOR C=10

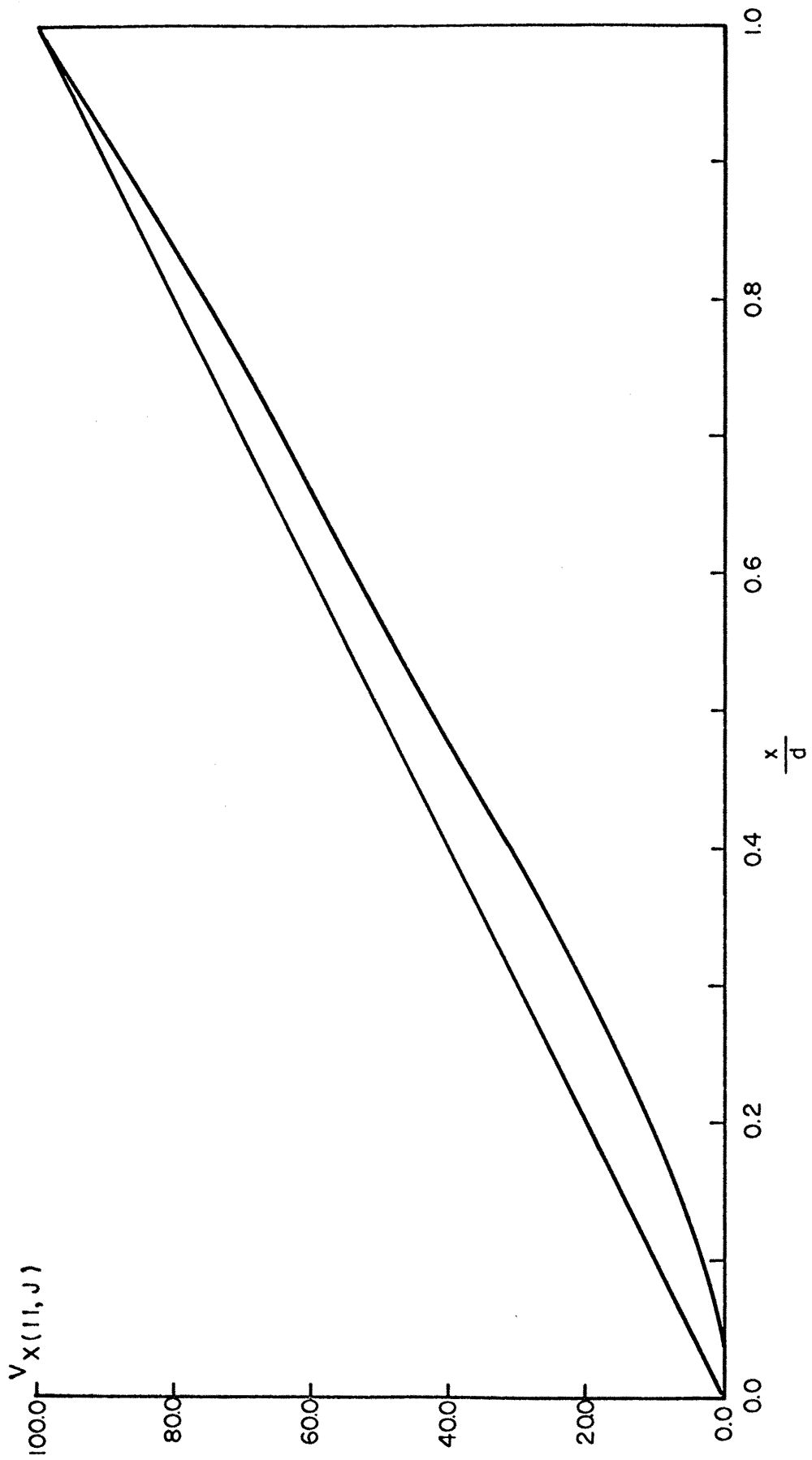


FIG. 7 POTENTIAL DISTRIBUTION AT THE CENTER OF THE SYSTEM

the space charges have zero initial velocity in the emitter. Thus, no potential-minimum exists between the electrodes. An increase of the emitter temperature would cause an increase of the emitted current, and therefore, this creates a "virtual cathode" with a minimum potential. The iterative procedure used here with $\rho = \frac{C}{\sqrt{U}}$ corresponds only to the "4/3 law", that is, only to the zone between the "virtual cathode" and the collector.

(II) The program for this case was changed, so that one of the points was held to a constant potential. The point chosen was the X(11, 6) and it was held to 50.0, that is, the value corresponding to the Laplace equation for that point.

For the control of the successive approximations, the point X(11,10) was chosen, that is, the point with the highest rate of change.

To improve the iteration and to estimate the errors, the number of iterations was increased to 50. Table III shows the new source program, the results of the computation and the potential lines. They also show the values of the point X(11,10), and the differences between the values of two consecutive iterations. Figures 10 and 11 show the corresponding graphs in function of the number of iterations. In Figure 10, it is possible to see that X(11,10) approaches the value of 2, and after 50 iterations it is possible to obtain results with less than 10% error, with respect to the end value. Figure 11 shows that the differences between successive iterations are so small

after 50 iterations that a much better result is obtainable only by increasing the number of iterations to 500, 1000 or more.

(III) Given a constant potential between emitter and collector, an increase of the emitter temperature produces a potential minimum close to the emitter. This can only occur when the emitted charges have an initial velocity (thermal velocity) different from zero.

The energy of the emitted charges may have a Maxwellian-distribution, and thus the potential function between emitter and potential minimum does not follow the "4/3 law", ("Childs-Langmuir-space-charge law" solved for the potential), considered above.

Only under the assumption of a uniform initial velocity, is it possible to make an approximation to the "4/3 law" in this zone.

The program shown in Table IV is similar to the one shown in Part (II). Here the evaluation of RHO, if $X(I,J)$ is negative, is modified. Figure 12 shows the potential lines for this case and Figure 13 the potential distribution in the center of the system.

TABLE III

C POISSON AND LAPLACE EQUATION IN SAME SPACE, DISTURBANCE,

```
DIMENSION X(21,11)
DO 1 I = 1,21
X(I,1) = 100.0
X(I,2) = 90.0
X(I,3) = 80.0
X(I,4) = 70.0
X(I,5) = 60.0
X(I,6) = 50.0
X(I,7) = 40.0
X(I,8) = 30.0
X(I,9) = 20.0
X(I,10) = 10.0
1 X(I,11) = 0.0
10 FORMAT (F6.3)
2 READ 10,A
DO 11 L = 1,50
3 FORMAT (F7.3)
PRINT 3, X(11,10)
DO 11 J = 2,10
DO 11 I = 2,20
X(11,6) = 50.0
IF (I-9) 18,5,6
5 C = A
GO TO 9
```

continued next page

TABLE III (cont'd)

```
6 IF (I-13) 5,5,18
18 RHO = 0.0
   GO TO 11
9 RHO = C*SQRTF (1.00/X(I,J))
11 X(I,J) = (X(I-1,J) + X(I+1,J) + X(I,J-1) + X(I,J+1) - RHO) / 4.0
   DO 13 J = 1,11
12 FORMAT (12F6.1)
13 PUNCH 12,X(1,J),X(2,J),X(3,J),X(4,J),X(5,J),X(6,J),X(7,J),X(8,J),
1 X(9,J),X(10,J),X(11,J),X(12,J)
14 GO TO 2
   END
```

TABLE III (cont'd)

POISSON EQUATION, DISTURBANCE $C = 10$

100.0	100.0	100.0	100.0	100.0	100.0	100.0	100.0	100.0	100.0	100.0	100.0
90.0	89.9	89.8	89.6	89.5	89.3	89.0	88.5	87.8	87.5	87.4	87.5
80.0	79.8	79.6	79.3	79.0	78.6	78.1	77.4	76.3	75.9	75.8	75.9
70.0	69.7	69.4	69.1	68.7	68.1	67.5	66.6	65.4	65.0	65.1	65.0
60.0	59.6	59.3	58.9	58.4	57.8	57.0	56.0	54.9	54.9	55.9	54.9
50.0	49.6	49.3	48.8	48.3	47.6	46.7	45.6	44.5	45.3	50.0	45.3
40.0	39.6	39.3	38.8	38.3	37.5	36.5	35.2	33.6	33.3	34.2	33.3
30.0	29.7	29.3	28.9	28.4	27.7	26.6	25.1	22.9	22.0	21.9	22.0
20.0	19.7	19.5	19.2	18.8	18.1	17.2	15.7	13.2	11.9	11.6	11.9
10.0	9.8	9.7	9.5	9.3	8.9	8.3	7.2	4.9	3.8	3.4	3.8
0.0	0.0	0.0	0.0	0.0	0.0	0.0	0.0	0.0	0.0	0.0	0.0

TABLE III
(cont'd)

ENTER DATA

C = 10

<u>X(11,10)</u>	<u>X(11,10) cont'd</u>
10.000	3.931
8.646	3.893
7.791	3.857
7.161	3.824
6.686	3.794
6.309	3.765
5.999	3.739
5.739	3.714
5.516	3.691
5.323	3.669
5.153	3.649
5.003	3.630
4.870	3.613
4.750	3.597
4.643	3.581
4.545	3.567
4.457	3.554
4.377	3.541
4.303	3.530
4.236	3.519
4.175	3.509
4.118	3.499
4.066	3.491
4.017	3.482
3.973	3.475

TABLE III
 (cont'd)
 C = 10

<u>X(11,10)</u>	<u>DIFFERENCE</u>	<u>X(11,10)cont'd</u>	<u>DIFFERENCE</u>
8.643			
7.781	1.357	3.259	0.070
7.141	0.862	3.195	0.066
6.651	0.640	3.134	0.064
6.256	0.490	3.076	0.061
5.926	0.395	3.020	0.058
5.643	0.330	2.966	0.056
5.396	0.283	2.914	0.054
5.177	0.247	2.864	0.052
4.980	0.219	2.815	0.050
4.802	0.197	2.768	0.049
4.641	0.178	2.722	0.047
4.492	0.161	2.678	0.046
4.356	0.149	2.635	0.044
4.229	0.136	2.593	0.043
4.111	0.127	2.552	0.042
4.002	0.118	2.512	0.041
3.899	0.109	2.473	0.040
3.803	0.103	2.434	0.039
3.712	0.096	2.397	0.039
3.626	0.091	2.359	0.036
3.545	0.086	2.323	0.038
3.468	0.081	2.286	0.036
3.395	0.077	2.250	0.037
3.325	0.073	2.215	0.035

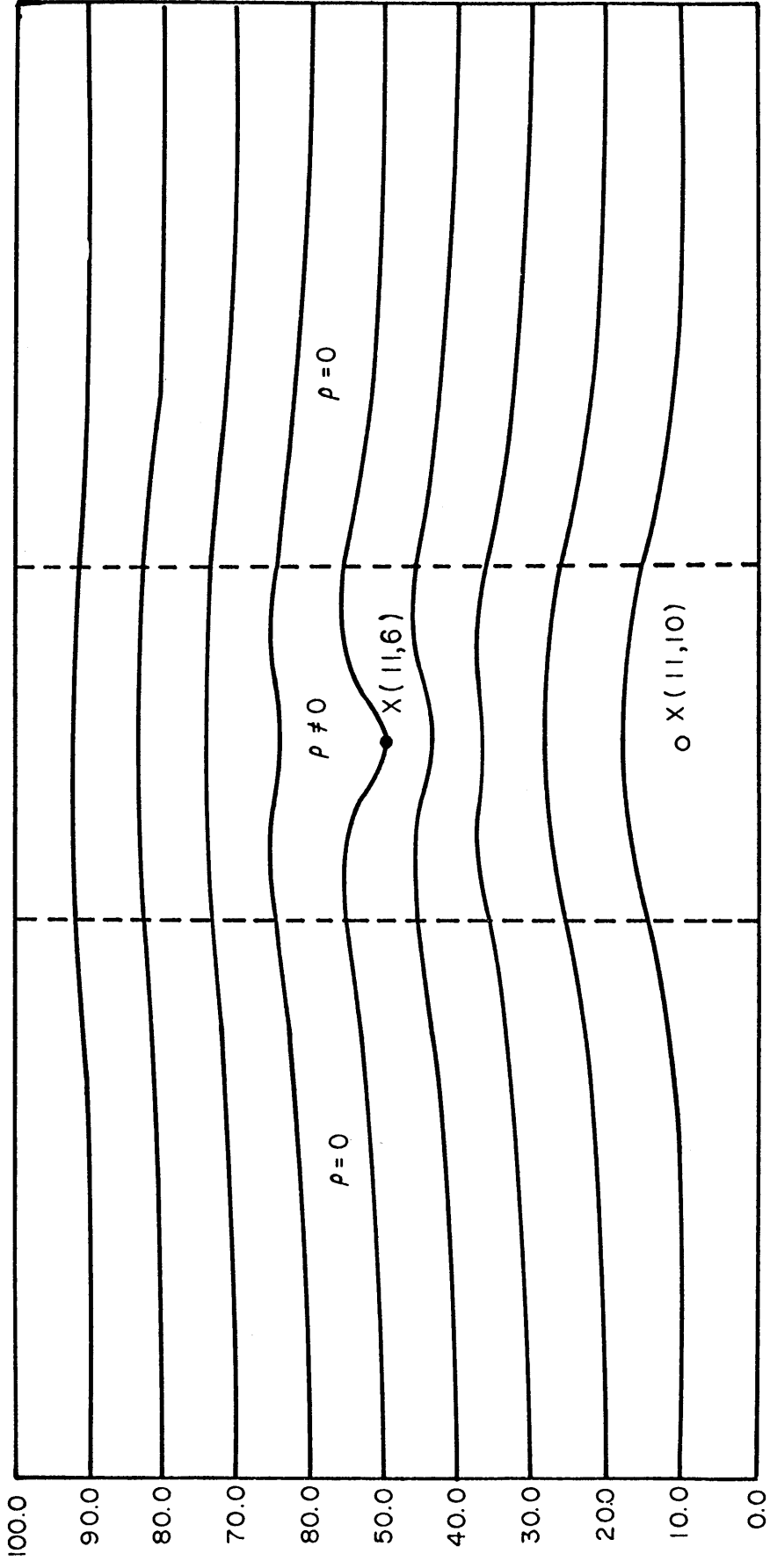


FIG. 8 POTENTIAL FIELD FOR C=10. PROGRAM (II)

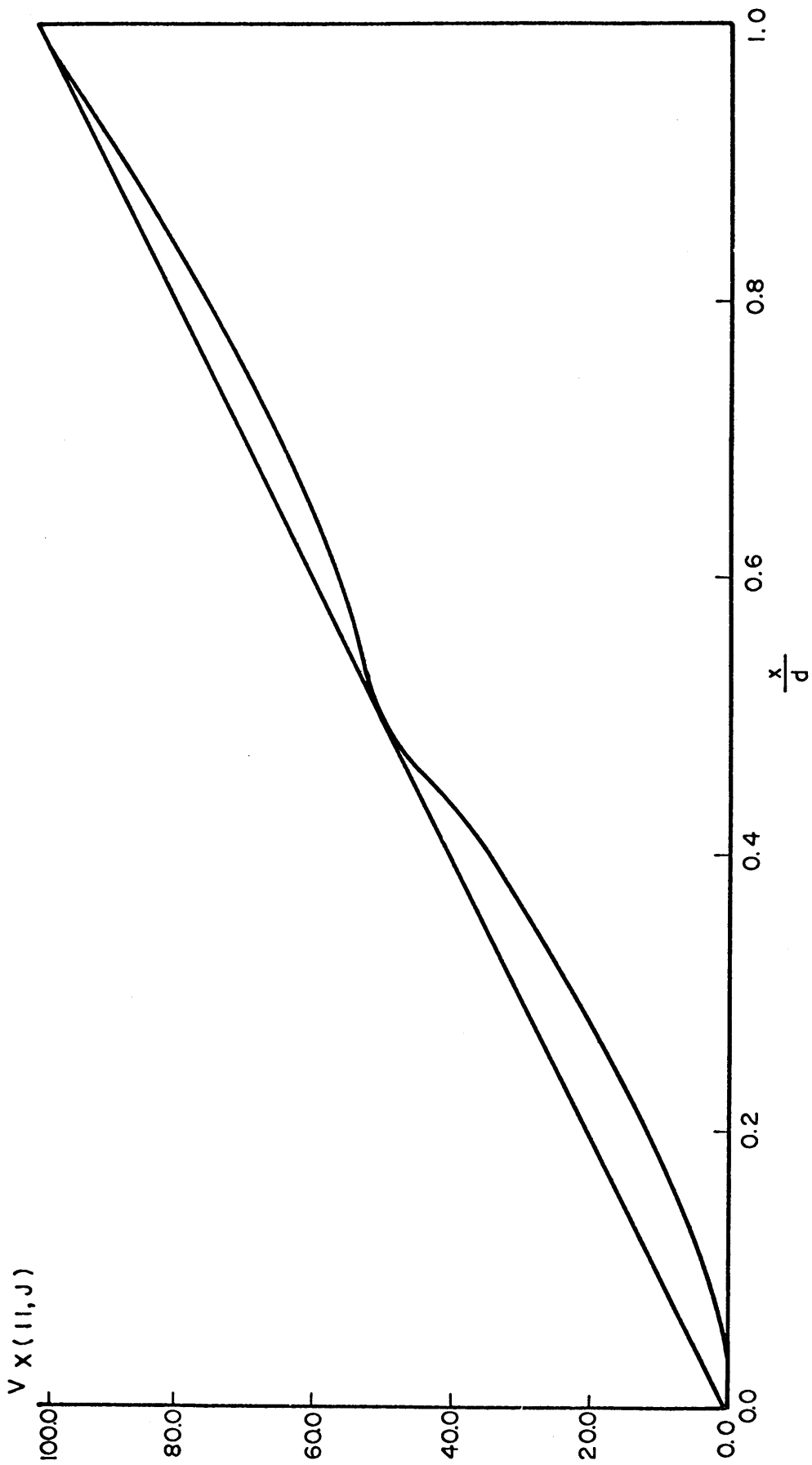


FIG. 9 POTENTIAL DISTRIBUTION. PROGRAM (II)

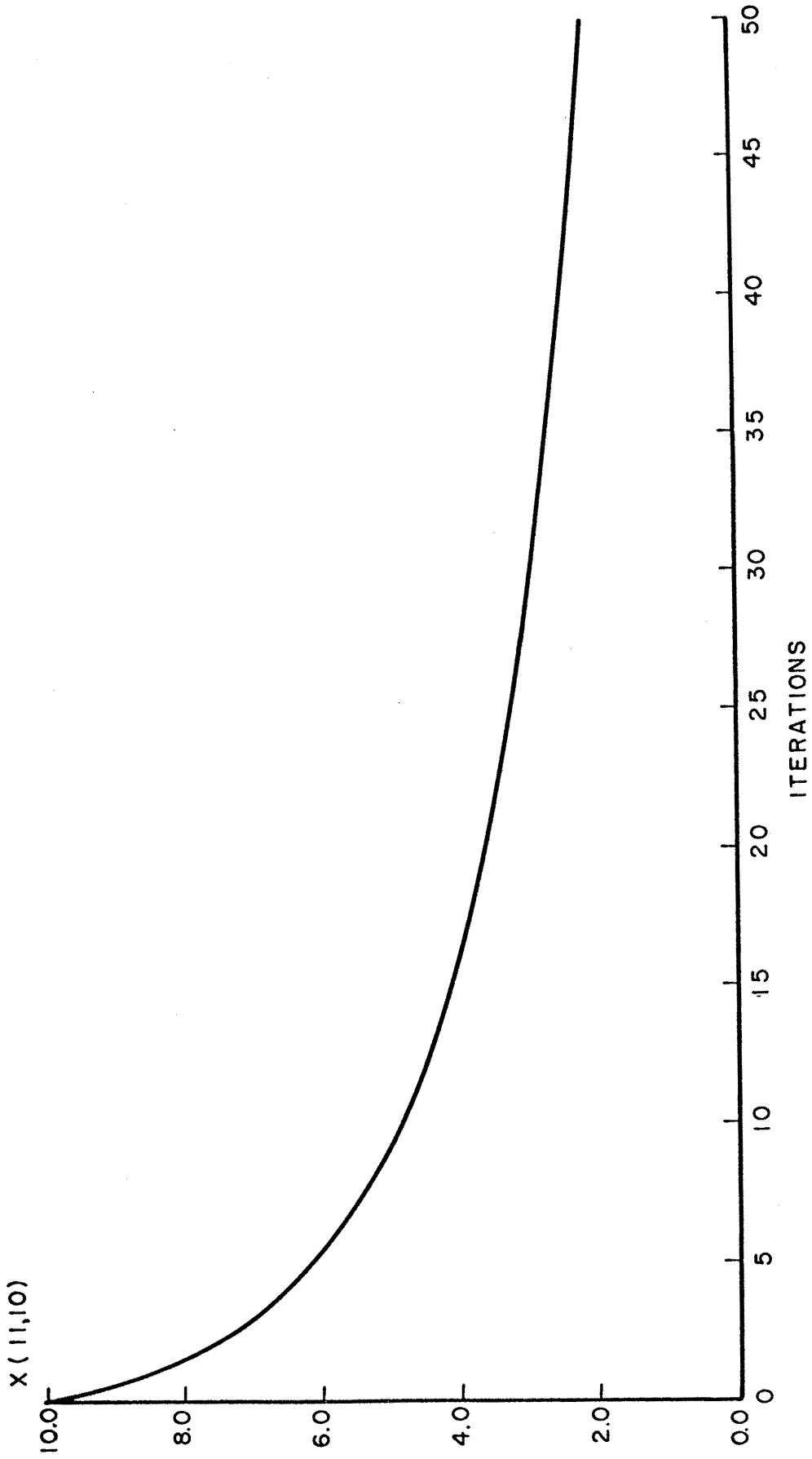


FIG. 10 VALUE OF X(11,10). PROGRAM (II)

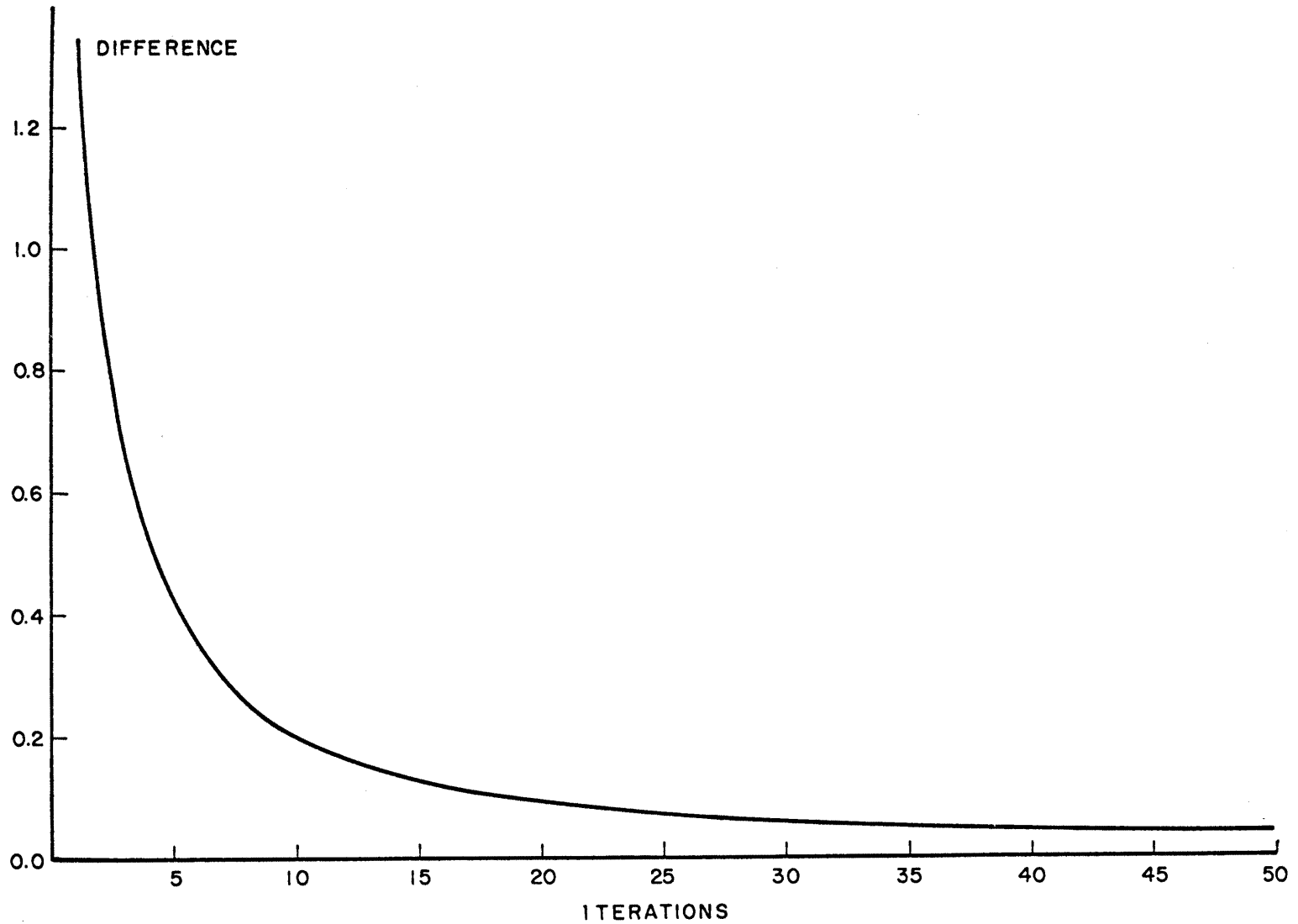


FIG. 11 RATE OF CHANGE OF X (11, 10). PROGRAM (II)

TABLE IV

C POISSON AND LAPLACE EQUATION IN SAME SPACE,
 C DISTURBANCE

```

    DIMENSION X(21,11)
    DO 1 I = 1,21
    X(I,1) = 100.0
    X(I,2) = 90.0
    X(I,3) = 80.0
    X(I,4) = 70.0
    X(I,5) = 60.0
    X(I,6) = 50.0
    X(I,7) = 40.0
    X(I,8) = 30.0
    X(I,9) = 20.0
    X(I,10) = 10.0
1    X(I,11) = 0.0
10   FORMAT (F6.3)
2    READ 10,A
    DO 11 L = 1,50
3    FORMAT (F7.3)
    PRINT 3, X(11,10)
    DO 11 J = 2,10
    DO 11 I = 2,20
    X(11,6) = 50.0
    IF (I-9) 18,5,6
5    C = A
    GO TO 9
  
```

TABLE IV (cont'd)

```

6  IF (I-13) 5,5,18
18  RHO = 0.0
    GO TO 11
9   IF (X(I,J)) 20,19,19
20  RHO = C*SQRTE(1.00/(-X(I,J)))
    GO TO 11
19  RHO = C*SQRTE(1.00/X(I,J))
11  X(I,J) = (X(I-1,J) + X(I+1,J) + X(I,J-1) + X(I,J+1) - RHO) / 4.0
    DO 13 J = 1,11
12  FORMAT (12F6.1)
13  PUNCH 12,X(1,J), X(2,J), X(3,J), X(4,J), X(5,J), X(6,J), X(7,J), X(8,J),
1   X(9,J), X(10,J), X(11,J), X(12,J)
14  GO TO 2
    END

```

TABLE IV (cont'd)

C = 15

ENTER DATA

10.000
7.969
6.613
5.552
4.679
3.912
3.196
2.480
1.691
.653
-1.759
-1.225
-2.170
-1.505
-2.212
-2.033
-2.140
-2.302
-2.549
-2.728
-2.708
-2.790
-3.008
-2.914
-2.982

ENTER DATA (cont'd)

-3.113
-3.138
-3.320
-3.530
-7.816
-4.556
-3.721
-13.352
-7.566
-5.104
-4.410
-4.405
-4.319
-4.499
-4.154
-4.339
-4.357
-4.151
-4.324
-4.250
-4.296
-4.241
-4.382
-4.133
-4.317

TABLE IV (cont'd)

POISSON EQUATION, DISTURBANCE

SECOND PROGRAM

C = 15

100.0	100.0	100.0	100.0	100.0	100.0	100.0	100.0	100.0	100.0	100.0	100.0
90.0	89.8	89.6	89.3	89.0	88.6	88.1	87.4	86.3	85.8	85.7	85.9
80.0	79.6	79.2	78.7	78.2	77.4	76.5	75.3	73.6	73.0	72.9	73.0
70.0	69.5	68.9	68.2	67.4	66.3	65.0	63.5	61.7	61.2	61.6	61.3
60.0	59.3	58.6	57.8	56.7	55.4	53.8	52.0	50.2	50.6	52.7	50.8
50.0	49.3	48.5	47.5	46.2	44.7	42.7	40.6	38.5	40.4	50.0	40.7
40.0	39.2	38.4	37.4	36.1	34.3	31.9	28.8	25.4	25.0	27.0	25.5
30.0	29.3	28.6	27.6	26.3	24.4	21.6	17.8	12.5	10.3	10.4	10.9
20.0	19.5	18.9	18.1	17.0	15.4	12.8	8.5	-.1	-1.6	-1.8	-1.2
10.0	9.7	9.4	8.9	8.3	7.3	5.7	2.9	-2.6	-4.0	-4.2	-3.7
0.0	0.0	0.0	0.0	0.0	0.0	0.0	0.0	0.0	0.0	0.0	0.0

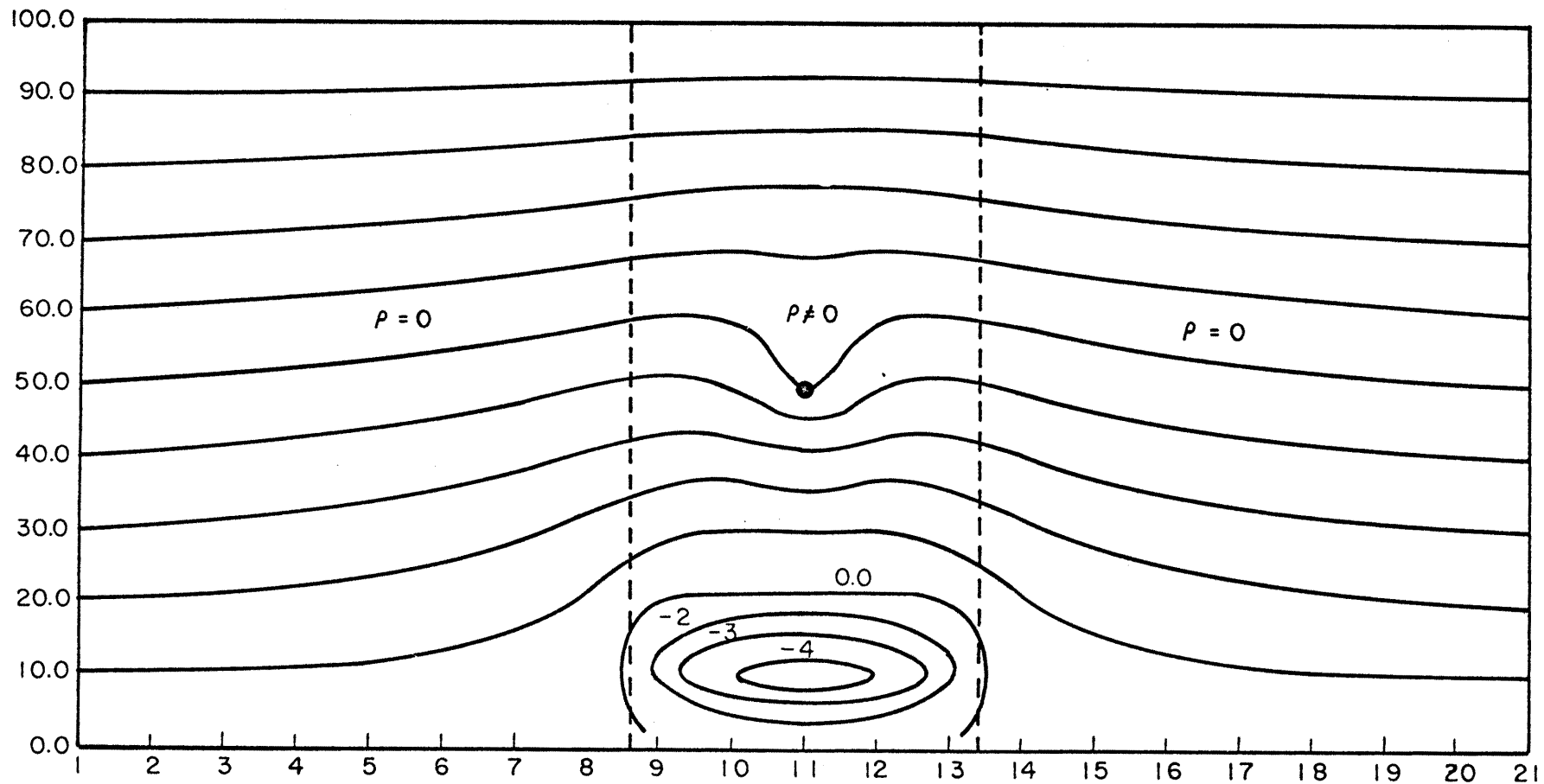


FIG. 12 POTENTIAL FIELD PROGRAM (III)

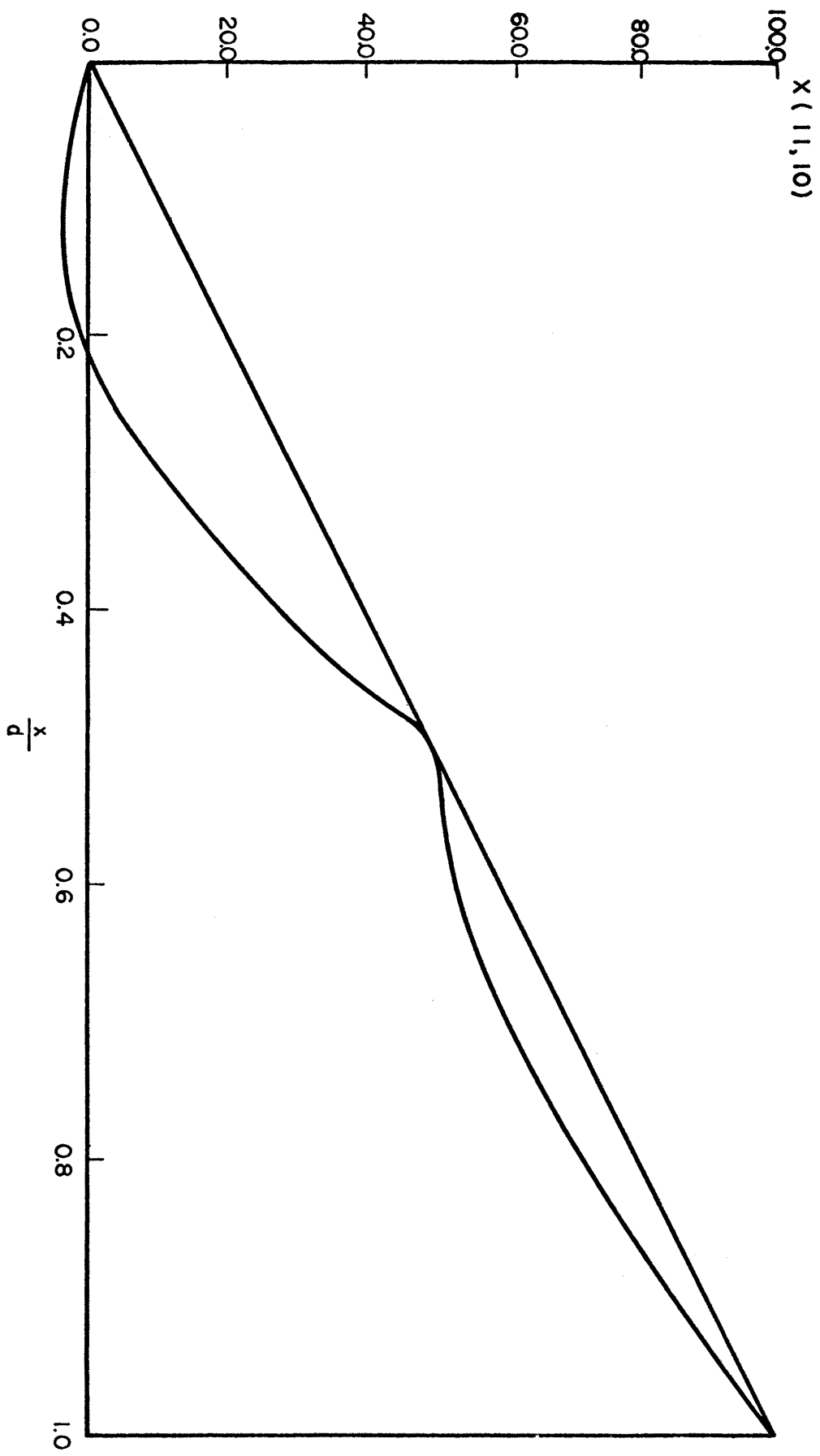


FIG. 13 POTENTIAL DISTRIBUTION PROGRAM (III)